

Electrodynamics in Iron and Steel

John Paul Wallace
Casting Analysis Corp.
(Dated: 2 June 2009)

Abstract

In order to calculate the reflected EM fields at low amplitudes in iron and steel, more must be understood about the nature of long wavelength excitations in these metals. A bulk piece of iron is a very complex material with microstructure, a split band structure, magnetic domains and crystallographic textures that affect domain orientation. Probing iron and other bulk ferromagnetic materials with weak reflected and transmitted inductive low frequency fields is an easy operation to perform but the responses are difficult to interpret because of the complexity and variety of the structures affected by the fields. First starting with a simple single coil induction measurement and classical EM calculation to show the error is grossly under estimating the measured response. Extending this experiment to measuring the transmission of the induced fields allows the extraction of three dispersion curves which define these internal fields. One dispersion curve yielded an exceedingly small effective mass of 1.8×10^{-39} kg ($1.3 \times 10^{-9}m_e$) for those spin waves. There is a second distinct dispersion curve more representative of the density function of a zero momentum bound state rather than a propagating wave. The third dispersion curve describes a magneto-elastic coupling to a very long wave length propagating mode. These experiments taken together display the characteristics of a high temperature Bose-Einstein like condensation that can be initiated by pumping two different states. A weak time dependent field drives the formation of coupled $J = 0$ spin wave pairs with the reduced effective mass reflecting the increased size of the coherent state. These field can dominate induction measurements well past the Curie temperature. *Single sensor and high temperature transmission data first presented as, Crystals for a Spin Wave Amplifier, at 20th Conference of Crystal growth and Epitaxy, AACGE/West, 6 June 2006, Fallen Leaf Lake, California.*

INTRODUCTION

This review of old data covers some neglected physics in the interpretation of low frequency reflection and transmission of weak inductive fields in ferromagnetic materials. Historically these experimental effects are not new and have been detected and reported as anomalously large permeability measurements of ferromagnetic material by a time dependent technique introduced by H. Rowland(1) in 1873 using a pair of inductors coupled by a ferromagnetic torus. Extending the technique to high temperature measurements of iron in 1910 by E.M. Terry(2) and measurements in high purity iron by R.M. Borzoth(3) 1937 produced values for permeability orders of magnitude greater than statically determined values. The details of the magnetic domain motion in the ferromagnetic torus were examined in 1949(4). The application of Ampere's law assuming no internal sources of time dependent fields other than the source inductor was the basis of this transformer design and application. Here a simplified form of this measurement is considered for isolating the material contributions to the responses that are not otherwise described by Ampere's law.

In addition, to my own problem of satisfactorily calibrating induction measurements on iron and steel to detect defects there is a set of other unanswered questions. The storage mechanisms involved in the operation of ferro resonant load leveling transformer patented by J. Sola(5) in 1954 require a more detailed explanation. The anomalous eddy current loss(6) which is a large effect for induction heating in Fe and FeSi alloys also has not been accurately described. Also, the steel corrosion inspection method "remote field testing" using slowly propagating, highly insensitive long range fields in low carbon steels(7) also requires an explanation. These unsolved problems coupled with the large conflict in the simplest experimental field reflection data to classical calculated values for ferromagnetic materials exhibits a weakness in our understanding. Ferromagnetism is a quantum mechanical phenomena, but a macroscopic connection to the field equations of Maxwell is essential to solving induction measurement problems. Since the time of Roland's introduction of the coupled transformer experiment, microscopic theories of elementary spin excitations have been developed to describe the temperature dependence of magnetization. The question of how a slowly varying time dependent induction $\mathbf{H}(t)$ interacts with individual spins, spin waves and structures such as magnetic domain boundaries (MDB) in iron and steel to produce the measured responses has remained an open question.

Spin wave theory developed as a lattice theory starting with considerations of the mechanics of a single one dimensional array of spins(8,9). These early works form the basis for the extensive investigations that have continued to the present. One difficulty in the application of a lattice theory to iron is that it does not include the local lattice relaxation dependence to the magnetization. This is a large effect in iron and can be seen in the fitted plot of lattice parameter as a function of temperature(10) through the Curie point in figure 1. In this plot the linear expansion with temperature is removed so the non linear response of the lattice to temperature variations taken through the Curie point become evident. The strains associated with the material below the Curie point are significant.

Spin waves and photons are the bosons that allow an exchange of spin states between carriers in ferromagnetic metal such as iron. These exchanges in addition to the transport of carriers are how the spin system is modified by the application of external fields and induced currents. These two classes of effects in addition to the lattice relaxation, phonon scattering, determines the measured responses and the various ways in which energy is distributed or radiates from the metal. Non saturated soft ferromagnetism that will be considered are

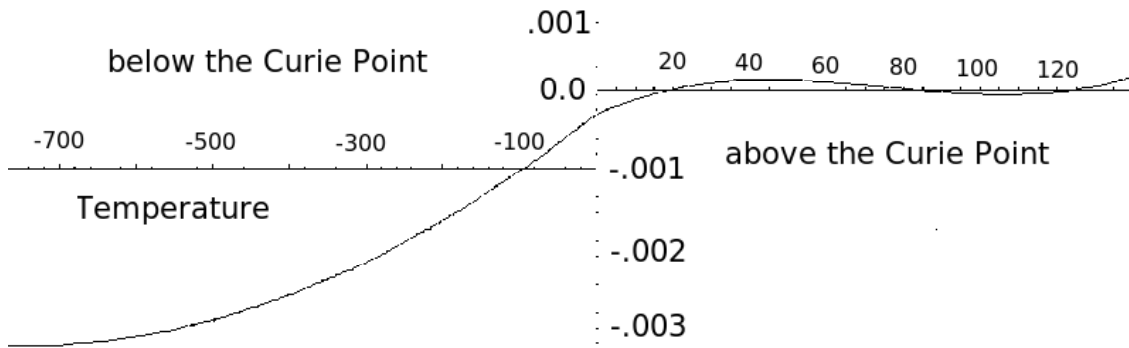


FIG. 1: Lattice parameter variations reduced from powder x-ray lattice parameter data for iron as a function of temperature with the linear thermal response removed. The temperatures are referenced from the Curie point. The displacements are in angstroms with the lattice parameter of iron being 2.86 angstroms at 30°C. The curve is similar to the saturation magnetization as a function of temperature. The total equivalent strain from room temperature to 770 C° is about .1% due to magnetic ordering.

partitioned by an array of MDB and the coupling between these regions will control the propagation of long range fields through the bulk of the sample. This couplings can be summaries in the first table.

Table 1: Field and Current Couplings

Region	Coupling	Details
bulk	strain or phonon	coupling to spin wave in limited freq. range
bulk	current	$\mathbf{j} \times \mathbf{m}$ spin wave generation
bulk	$\mathbf{H}(\omega)$	field couples action across MDBs
MDB	current	electron transport across MDB generate spin waves
MDB	spin wave	emission and capture across MDB move MDB
MDB	photon	emission and capture across MDB move MDB
Surface	photon	emission and capture with spin waves

In iron these 6 process are active at once. Iron's split band structure(11) allows for direct transitions between electronic spin states, that are not available in the other ferromagnetic transition metals and provides another source for non thermal spin waves. None of these fields are long range fields within a ferromagnetic metal.

ANALYSIS IN WEAK FIELDS

The construction of the Rowland transformer is too complex to allow a simple closed form analysis to represent the experiment. You have to eliminate the bends to get a simple

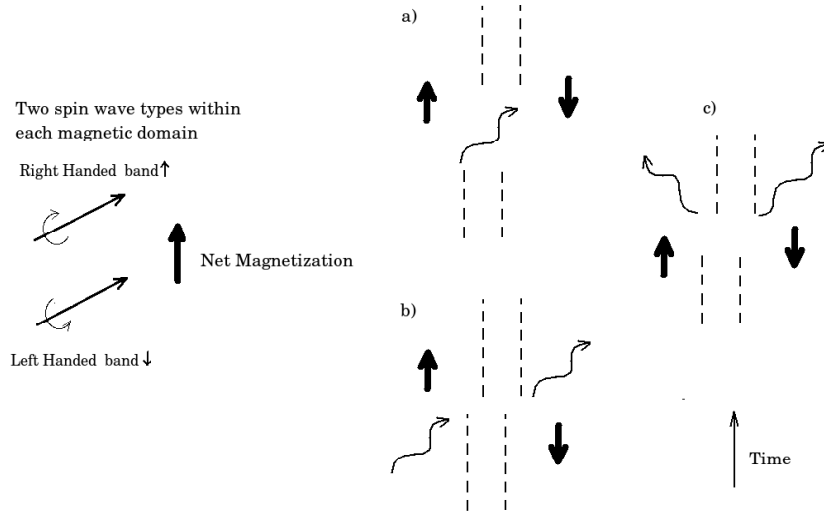


FIG. 2: **Graphic of the principal transitions that can generate a non thermal boson population. The magnetic domain boundaries are shown as broken parallel lines. For iron which has two spin bands, there are more paths available to pump the spin wave population such as shown in figure 2c which s requires a spin wave on each band to be emitted.**

experimental apparatus with a source inductor around a cylinder and a receiving inductor either being the same inductor, figure 3a, or a displaced inductor, figure 3b. These geometries allows the EM boundary value problem to be easily solved in closed form using only assumptions of material homogeneity.

Our first measurements are for weak time dependent fields with long free space wavelengths that will act as a small perturbation on iron's spin system. For the applied induction field interacting with a ferromagnetic conductor there are three regions in the material that influence the interaction. The first is a near surface where some domain motion is inhibited by the effect of the surface to minimize leakage fields. The next deeper region penetrated by the induction field can drive domain motion more easily. Finally, there is the bulk interior below the electromagnetic skin depth where any measurable transverse propagating fields vanish.

All the measurements described are macroscopic measurements on physically large samples when compared to grain size, electronic mean free path and the conductors electromagnetic skin depths. These measurements are on a small scale when compared to free space electromagnetic wavelengths and acoustical wavelengths of the fields at the applied frequency.

The measurements made here will represent one of a set of experiments that will isolate the non classical effects that are common and easily detectable at low levels with low frequency, time-dependent fields that interact with ferromagnetic conductors and insulators.

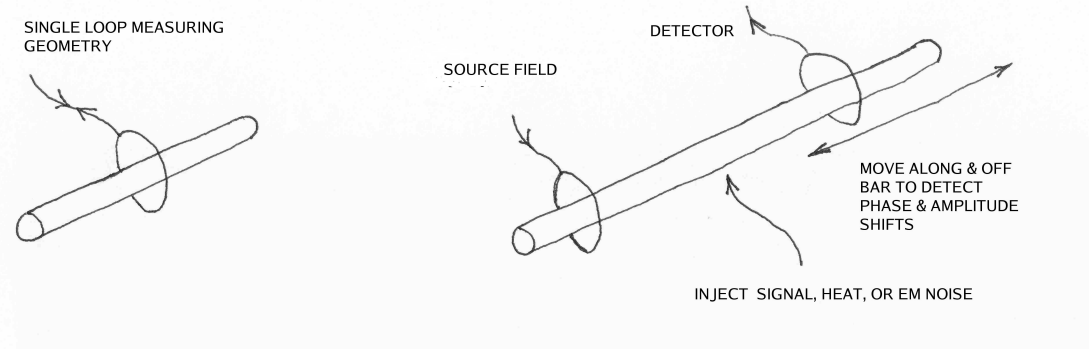


FIG. 3: a) Single sensor encircling , b) Dual coil transmission measurement with possible second source injection.

CALIBRATION OF INDUCTION MEASUREMENTS

The principle technique used here is often referred to AC magnetic susceptibility measurements and this is a label which is misleading. For simple conductors the technique is very powerful and accurate in reducing measured reflections to structural and electrical conductivity profiles. For magnetic material this technique must assume a magnetic constitutive relation that may not be accurate or adequate. Therefore, these measurements will simply be called induction measurements with an analysis based on a macroscopic set of Maxwell's equations.

An induction measurement system consists of two parts. A network that supplies and detects the field and the sensor which is usually a coil. This coupled system is calibrated as a complete system. The calibration requires the measurement of a standard of known properties in a computable boundary value geometry that reduces the standard to a calculable response. The electromagnetic induction boundary value problem was solved in closed form for selected geometries by Dodd and Deeds(12) in the low frequency range below 10 MHz for typical metallic conductors. In the quasi-static approximation for conductivity these solutions are accurate for simple conductors such as copper, where the electronic mean free path is short relative to the structure of the sample being measured(13). This allowed induction measurement of non ferromagnetic conductors to produce precise dimensional and conductivity measurements at ambient(14) and at high temperatures.

What follows is a simple calibration scheme for the fields which can be thought of as an analog to optical reflection. In order, to do induction studies of high temperature materials, crystal growth processes a simple calibration technique was introduced(15) where a known conductivity standard is compared to an unknown sample. Calibration was reduced to practice when complex arithmetic could be done on a microprocessor(16) to allow the mapping of a signal space into a measurement space. This essentially removes the details of the network that connected the source and receivers so long as they are operated in a linear response region well below any self resonance of the measurement system. This in effect removes the measurement system by the calibration in using a two dimensional transformation matrix for each frequency of measurement. Extending this calibrated measurement technique to ferromagnetic systems such as carbon steels, pure iron, cast irons, ferromagnetic ore bodies, ferromagnetic amorphous metals, ferro fluids and composite ferromagnetic material produces results that conflict with simple magnetic models. The assumption required

for electrical conduction analysis is quasi-static approximation and with ferromagnetic material this assumption is insufficient. The quasi-static approximation for electron scattering in conduction does not have an analogue when considering a system of ferromagnetic spins and their response to a time dependent field.

For example the simple geometry, figure 3, of measurement and analysis is a single turn induction loop used both as a source and receiver surrounding a right circular cylinder of copper or a well annealed iron. Solving the boundary value problem of the wave equation for the vector potential, \mathbf{A} , in a source free region such as the interior of a conductor will yield the local electric and magnetic fields through the vector potential. The field equation in the source free region where we have used the definition $\mathbf{B} = \mu\mathbf{H}$ is simply:

$$\nabla^2 \mathbf{A} - \sigma\mu \frac{\partial \mathbf{A}}{\partial t} - \epsilon\mu \frac{\partial^2 \mathbf{A}}{\partial t^2} = 0 \quad [1]$$

The above expression is easily solved by maintaining the continuity of both the electric field, \mathbf{E} and the magnetic induction, \mathbf{H} , at each boundary for either one or two dimensions with multiple layers.

The known properties of the measurement are the signal level, frequencies, the diameter of the loop inductor and the diameter of the bars under test. If a conductor of known purity, dimension and temperature is used as a standard one can capture the complex signal as reflected from this standard $S_m = (x_m, y_m)$ and also compute the reflected response, $S_c = (x_c, y_c)$. The computed value of the reflection is found by solving the boundary value problem. One can compute a 2×2 matrix \mathbf{T} , that connects these two vectors.

$$S_c = \mathbf{T}S_m \quad [2]$$

A simple example with the source normalized to $S_{source} = (1, 0)$, then a perfect conductor filling an encircling loop will produce a response of $S_c(\sigma \rightarrow \infty) = (-1, 0)$ and for an empty sensor $S_c = (0, 0)$. For subsequent measurements, S_m , the application of the matrix \mathbf{T} , transfers the signal vector into a space that can be interpreted, R .

$$R = \mathbf{T}S_m \quad [3]$$

It is useful to consider the limits of these measurements and responses in a simple experiment. With fixed coil or loop surrounding a cylindrical conductor the response $R(\sigma)$ where σ is the conductivity will obey this relationship,

$$K = \frac{|R(\sigma)|}{|R(\sigma \rightarrow \infty)|} < 1 \quad [4]$$

This can be shown by solving the boundary value problem and observing the behavior of the responses by taking the cylinder's conductivity to infinity. This is simple to show either for a long encircling coil about a cylinder, a plane wave on an infinite plane reflector or a single loop surrounding a cylinder. Similarly if the material permeability is examined in the same way the result are the same. There can be no measured reflected signal that was greater than initially supplied. This is easy to prove in any geometry. This is because the propagation vector in the material contains a product of σ and μ and even if complex the limiting relations of equation 4 and 5 remain true.

$$\frac{|R(\sigma, \mu)|}{|R(\sigma \rightarrow \infty, \mu_o)|} \leq 1 \quad [5]$$

An example of this type of computation for a simple one dimensional reflection deriving the upper bound on K is located in appendix A. At low field levels equation 4 can be understood as a statement of the dissipation as a result of material resistivity. The denominator is the response of a very good conductor. The numerator describes a similar sample where we are increasing the permeability possibly by increasing the sample temperature. Equation 5, however, is only a result of solving Maxwell's equation using the simple linear magnetic equation of state,

$$\mathbf{B} = \mu\mathbf{H} \quad [6]$$

The weakness in this model description of a ferromagnetic material is apparent when the ratio K is measured at values greater than 1. This solution is analogous to any optical reflection where the reflected amplitude is always less than or equal to the incident source.

In a good conductor the one dimensional cylindrical solutions are quite accurate for a long sensor because the fall off in fields at the coil ends are abrupt, $\frac{1}{r^4}$. Where r is the distance from the end of the coil. This rapid decrease results from the cancelation of the fields due to the out of phase induced field in the conductor. So standards are typically taken with high conductivity non magnetic materials.

MEASUREMENTS

The effects to be examined here are the reflection of an imposed time varying field on various ferromagnetic materials. In addition the transmission of a signal generated from a time varying field will also be examined. Particularly, the penetration of signal well beyond the electromagnetic skin depth in soft ferromagnetic conductors. The analysis is strictly macroscopic with the aim of determining the changes required in the application of Maxwell's equation in order to physically understand the responses. The equipment used evolved from early multi frequency eddy current instruments used on stainless weld measurements(17) where the response of minority delta ferrite and solidifying cast irons(18) were monitored for phase and magnetic transformations. The signal generation and detections system used in the current measurements is a Process Monitor IV from Casting Analysis Corp. which has three quadrature phase detectors that can provide three signal sources that operate independently. All detectors use a common master clock which maintains a uniform phase relation in time among all channels. The system can feed all three signals into either a single or multiple coils that can be detected on any three channels. The operating frequency range is from 1 Hz to 20 MHz. Typically this instrument is used for multi frequency direct inversion of calibrated eddy current data for monitoring properties over a wide temperature range such as crystal growth. The free channel is used for spectrum scanning assuring that the system is operating in linear range where there is not a measurable $2f$ or $3f$ harmonic from the sample.

The operating software can compute the boundary value problem in the geometries that are used in the following experiments as a long solenoid and a single loop. The quadrature responses are computed for the standard and then data taken on that standard is used to compute the matrix \mathbf{T}_i for each frequency, ω_i of measurement. This allows single or multiple frequency reflection measurements to be made along with transmission measurements. When taking transmission measurements the calibration uses the sample under test as the standard or no sample with the source and receiver as close as possible. This results in a reference

at a phase angle of 0° so that measurements on the bar produce the total phase shift as referenced to 0° or the source. The typical maximum drive are 10-20 milliamperes for the reflection experiments into 12 turn coils 1.5 cm in diameter and 1.5 cm long. These coils are driven in series with a 51 ohm resistor. The sample diameter determines the local maximum for the field. All detector coils are terminated with a 51 ohm resistor to ground. The detector coils are the same construction as the probe drive coils. The current levels are set at least an order of magnitude below where we cannot detect non linear components in high purity well annealed iron when two different frequencies are used to drive the source. The linear behavior of the system acting on copper is confirmed experimentally in data taking with increasing current inputs showing a well behaved response as shown in figure 4. The behavior for iron is different with a response increasing monotonically with the drive level in the same figure.

Simple Cylindrical Boundary Value Reflection Experiment and Analysis

The first experiment is a simple reflection measurement in the cylindrical geometry for a set of standard materials when the source and sensor are the same, show the non classical behavior of the detected amplitude to the applied signal. For a magnetic material with $\mu > 1$ the value of \mathbf{K} should be less than 1, however, the two magnetic materials measured show values between 22 and 35. This is a very large error, greater than 2000% for the application of a simple constitutive relation, $\mathbf{B} = \mu\mathbf{H}$.

The simplest reflection experimental data is recorded in figure 4 which shows the signal for 3 samples at two different frequencies while the source drive level is increased. The key point to take from this data is that for soft ferromagnetic conductors and insulators there is measured a significant signal energy above the applied level. As shown previously, it is not possible to get a result found in figures 3 or 4 by varying μ in the complex plane. There is also no apparent resonances detected in the frequency range as shown in figure 4.

The apparent enhanced level measured at the applied frequency is not a peaked resonance as one would find in an oscillator associated with a local physical property; because if the frequency is decreased, there will be a slow increase in the amplitude. By using $\mathbf{B} = \mu\mathbf{H}$ there is not a way to compute a return amplitude greater than 1. Since ferromagnetism is a quantum mechanical phenomenon there is not any reason to assume that the macroscopic field should be proportional to the applied induction. These large signals also indicate we do not have accurate knowledge of the spatial distribution of the fields within the cylinder.

Radial Scale Independent Measurement of Long Solenoidal Reflection

To gain more understanding of the difference of a ferromagnetic material such as iron to a simple conductor such as copper in the response, it is easy to remove the radial scale dependence from the problem of figure 3a to get a material response that is independent of the radius of the sample for a known applied field. If the material behaves as a simple reflector with Joule dissipation of the induced currents the reflection now should be independent of the sample's radius. The boundary value problem for the continuity of the electric field, \mathbf{E} and the magnetic induction \mathbf{H} result in a pair of equations at the boundary of a homogeneous cylinder radius, r , where k_o is the free space propagation vector.

K Signal/Max Classical Response

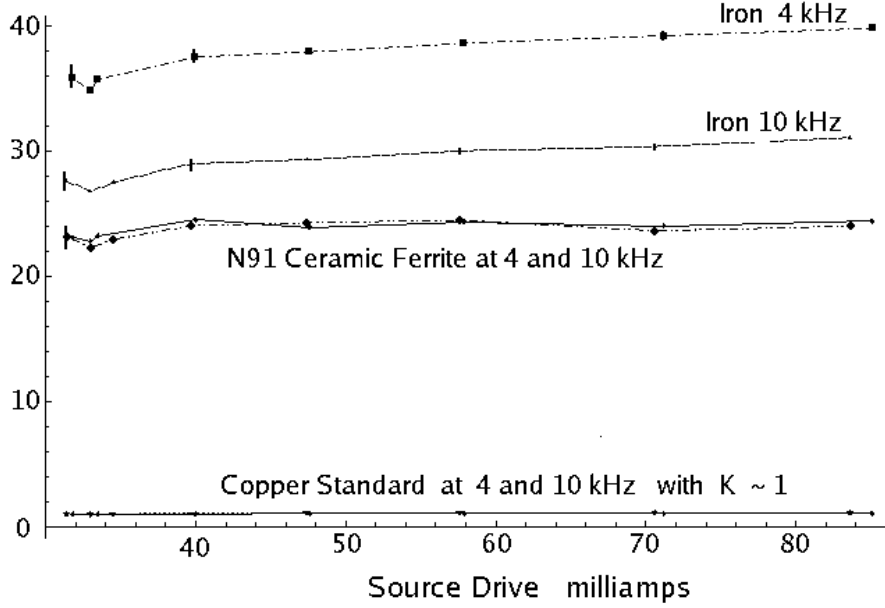


FIG. 4: Single sensor measurements of reflected eddy current response in copper, iron and a NiZn ferrite. The key feature is that the ferromagnetic samples all have $K \gg 1$. In iron's case this value approaches 40. The iron in this case was of 99.99% purity and held for greater than 30 days at 1050 C° in flowing hydrogen and then furnace cooled to reduce the interstitial content. Iron differs from the other samples in that there is a signal increase as a function of drive current which is not the case for copper or the ferrite. This nonlinearity is also not predicted by the classical modeling in the boundary value problem. The variations at low current levels are caused by low signal level for the copper standard resulting in reduced precision. In this experiment field levels range up from 10^{-7} Tesla.

$$AJ_1(k_or) + BY_1(k_or) = CI_1(kr) \quad [7]$$

$$\frac{1}{\mu_o}(AJ'_1(k_or) + BY'_1(k_or)) = \frac{C}{\mu}I'_1(kr) \quad [8]$$

If the source coil has a radius, r_c , with a source field $AJ_1(k_or)$ we can consider the field at the surface of the cylinder is normalized by the ratio $J_1(k_or)/J_1(k_orc)$ and similarly the response from the cylinder is normalized by the ratio $Y_1(k_orc)/Y_1(k_or)$. The measured responses, S , amplitude is then found in the scale independent form, S_n as:

$$S_n = S \frac{J_1(k_orc)Y_1(k_or)}{J_1(k_or)Y_1(k_orc)} \quad [9]$$

Taking data on some annealed low carbon steel and copper of different radii at 10 kHz illustrates the difference in the materials' responses.

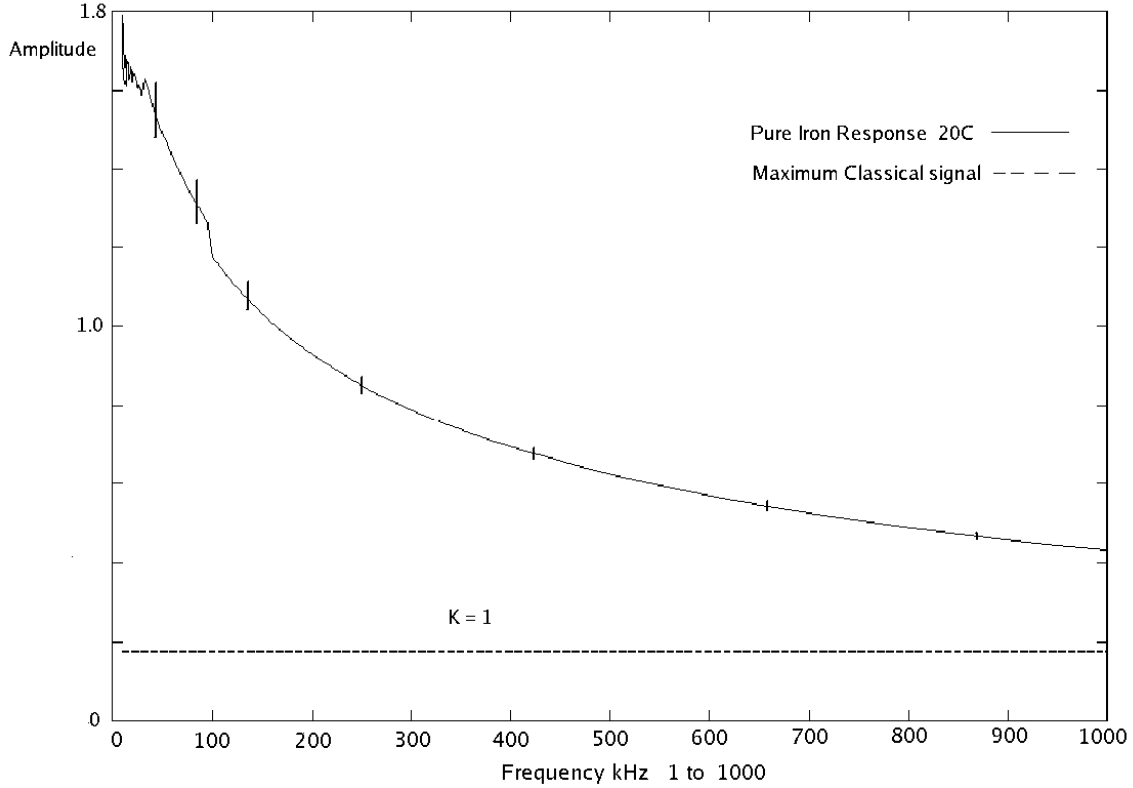


FIG. 5: Single sensor measurements of amplitude plotted as a function of frequency in high purity iron. Three separately calibrated sweeps are joined to cover the frequency range, and the offsets observed are from joining data together. The noise at low frequencies is due to less resolution for the calibration measurement on copper which is used to normalize the data to assembling the sweep on one scale.

Table 2: Scale Independent Response with A Long Solenoid for Copper and hot rolled 1018 steel, 10 kHz coil 7.85mm Radius. The raw measured signals in Copper fall fast as the radius is reduced. The radially independent signal for copper is flat. The signals actually grow in the hot rolled 1020 steel as the radius reduces.

Cu Radius mm	S \pm .007	S_n	Fe Radius mm	S \pm .007	S_n
4.75	.319	.87	5.85	2.00	3.60
4.25	.263	.89	4.85	1.54	4.03
1.55	.027	.7	3.95	1.276	5.04
			2.65	.888	7.79

The main feature of table 2 is that copper’s response is nearly independent of radius and the signal for the iron data is large and growing with decreasing radius. The result is an increasing signal with reduction of radius where the ohmic loss effects have already been corrected as a function of radius. As the radius decreases, the path for losses out the ends is reduced.

The practical coupling of fields to ferrous cores in transformer design illustrates some advantages for weak time dependent field when increasing the surface area relative to volume. It is not apparent that the traditional explanation of eddy current losses play much of a role in this optimization for more area per unit volume in a ferrous core for weak fields.

Saturation Effects on Transmission and Local Signal Level

One simple experiment that can be performed in measuring the locally reflected field from a cylindrical sample is to apply an axial static magnetic field of a few hundred gauss from a ceramic permanent magnetic with a central hole in which a sample can be placed with a coaxial coil, figure 3a. This has the main effect of removing a significant fraction of MDB and aligning the static magnetization within the material. The effect on the local signal shows a large difference in the soft magnetic materials. The locally measured signal and the responses with and without a static axial magnetic field are listed below. **Table 3:**

Static magnetic field effect on the reflection for 50 kHz signal. The error bars on phase $\pm.02^\circ$ and amplitude $\pm.002$.

Material	phase ϕ	change in phase	% amplitude reduction
Fe	-39.7°	-35°	87.5%
Ni	-84°	-63°	30%
Co	-81°	-29°	27.5%
Ferrite N91	-2.7°	$+1.5^\circ$	96.2%

The phase data shows the metals Ni and Co with the saturating fields decrease with partial saturation. The Ni and Co are from machined bar stock and not annealed whereas the Fe sample is a well annealed specimen with very low interstitial impurity content. For a simple conductor the phase angles fall between $-90^\circ > \phi > -180^\circ$ whereas for a ferromagnetic insulator like N91 the phase angle will approach 0° or $S_m = (amplitude, 0)$ for a response vector. The static \mathbf{B} field is not quite strong enough to push the phase angle response of Fe to values as low as -90° . The NiZn, N91, ferrite is the softest of the materials and whose amplitude is greatly effected, but its phase is driven towards 0° which is indicative of a more highly permeable insulating material phase response for a classically describe magnetic material. The iron and the ferrite amplitude response are well beyond what one would calculate as the limiting response for a classical reflection without the static field. With the static field the phase angles fall into better agreement with a classical analysis. The result of minimization of MDB area or immobilizing MDB on microstructural features from cold work acts similarly by removing a significant portion of the nonclassical response.

PROPAGATING WEAK FIELD MEASUREMENTS

For propagating fields our first measurements are for weak time varying fields with long free space wavelengths that will act as a small perturbation on the iron. We are within a small fraction of the free space wavelength at the source field for the entire frequency range being examined. The dispersion of the components that produce the measured excesses in the reflection responses may allow the individual sources and propagation modes to be

isolated and identified. By scanning the displacement of the receiver as well as the frequency of the source, the overlapping effects that occur with a single driven sensor/receiver can be partially lifted.

Calibrating the transmission standards is much simpler because it can be a differential measurement from the position of closest approach of the source and receiver normalized to a signal vector $S = (1, 0)$. The first component representing the magnitude of the component in phase with the source and the second component is the amplitude of the signal that is phase shifted -90° to the source. The zero point is established by removing the drive signal from the source. This allows the differential phase change to be acquired accurately with displacement. An absolute calibration can be made by removing the medium and measuring the source field directly as is done in the single sensor measurement. The amplitude responses are scaled to the normalized source amplitude at the closest approach. This allows a direct measurement of the fields decay as a function of displacement.

In the transmission experiments, figure 3b, the coil drives are typically 30 milliamperes into 10 turn coil 1.3 cm in diameter and .9 cm long, driven through a 10 ohm series resistor. The sample diameter determines the local maximum for the field which can be easily computed. The detector coil is the same as the source coil and is terminated with a 51 ohm resistor to ground and it feeds a transformer input on the Process Monitor IV. In translation measurements for the extraction of the dispersion curves Process Monitor IV steps the probe down the bar taking readings every .05 mm while running at a single frequency for each scan. When selecting a frequency to work at in the transmission mode a frequency sweep should be made with the source off to determine if there are any extraneous signal sources being sensed.

First Transmission Measurement

From the literature it is known that induction formed propagating fields in iron and steels exist(7). Also we have a great deal of data(19) on the high temperature measurements of steels with a single probe which shows a significant enhancement of the field levels above what we measure at room temperature. An example of this is shown in figure 6. The other features of the high temperature data are the constant phase value as one approaches the Curie point and the decreasing noise level detected in the large reflected response. In the example in figure 6 the signal increase is by a factor of 6 moving to the Curie point. The phase drops at the Curie point to a value expected of a conductor at above 770°C .

The question posed here is whether transmission will be possible in a region where the steel is raised above the Curie point? This transmission experiment depends on two processes, first is generating the field and the second is the role the medium plays in its motion. This immediately would reveal whether the signal could survive in a paramagnetic region of no permanent magnetic moment but a spin wave population and no magnetic domain structure. If the field traversed that region then it answered one question about the necessary medium required for transmission of the signal. This first experiment was done on a 4.7 mm diameter rod 1018 hot rolled steel. The coils were 11 turns mounted on water cooled copper mono turn rings and 8 mm long. The calibration was based on the source and receiver coils empty and far removed for a zero point. Then the coils brought close together axially for taking the 0° phase and amplitude reference. So that all subsequent measurements are referred to these measurements and the phase delays are absolute and caused by the material.

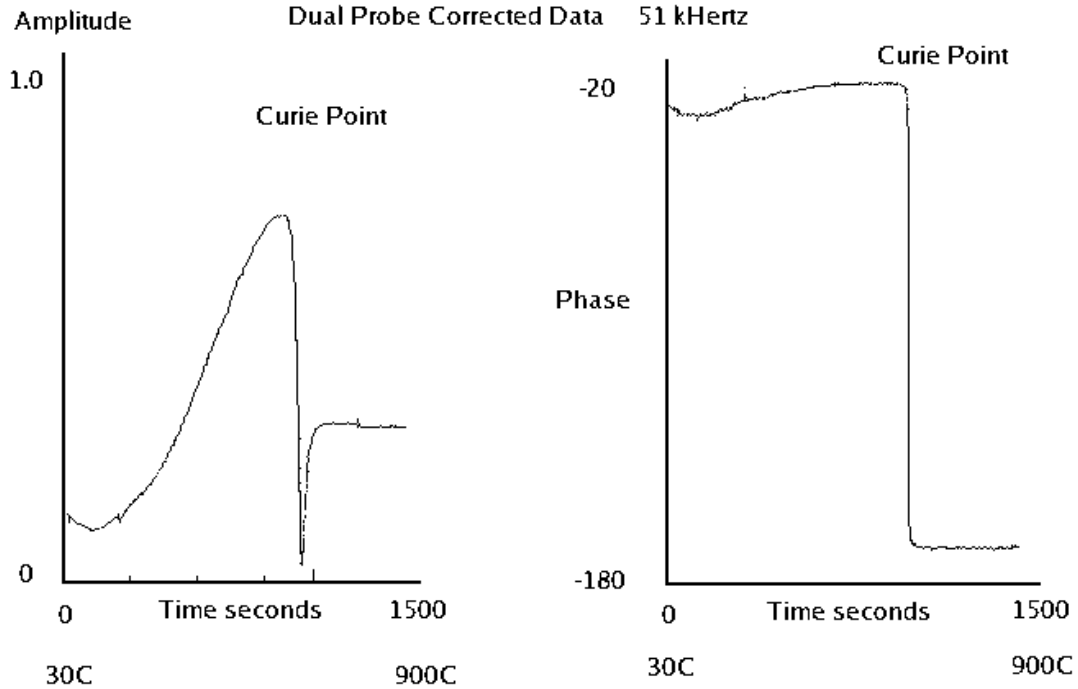


FIG. 6: Single sensor on iron at 51 kHz, heated from 30 C to > 900 C reflected amplitude response on the 0° axis. Data taken on a Process Monitor II in a low carbon steel.

The transmission data for phase and amplitude with the heated center are shown in figure 7 and 8 respectively. In the vicinity of the Curie point there was a rapid increase in the phase delay along with a step increase in response. Then as the center region passes through the Curie point the transmission level abruptly drops, not to zero, but to value that still shows a transmission response double that of the room temperature value. This response is made up of a combination of the gain in the heated rod below the Curie point and the loss in the region above the Curie point. The phase delay suffers a significant reduction with the section above the Curie temperatures. The transition through the Curie point arrests a portion of the propagating field but from a classical EM analysis the attenuation is too weak and the phase response is of the wrong sign. That is if an axial induction at 10 kHz is impressed on a conductor it is rapidly attenuated on the order of 1 mm and its phase is significantly delayed and not advanced. Whereas the single coil heating experiment of figure 6 shows nothing unusual and differing from a classical EM response above the Curie point. Generation of the excess signals seen below the Curie point both in the transmission and single sensor data are not explained by a classical analysis.

The frequency dependence of the transmission drop at the Curie point is shown in table below for a set data take with the identical set up as just described but with a transmission distance of 14.5 cm and a heated zone of 2 cm.

Table 4: Signal transmission through at 2 cm long hot zone with a spacing between transmitting coil and receiver of 14.5 cm. The phase decrease error bars, are approximately 10 % of the value.

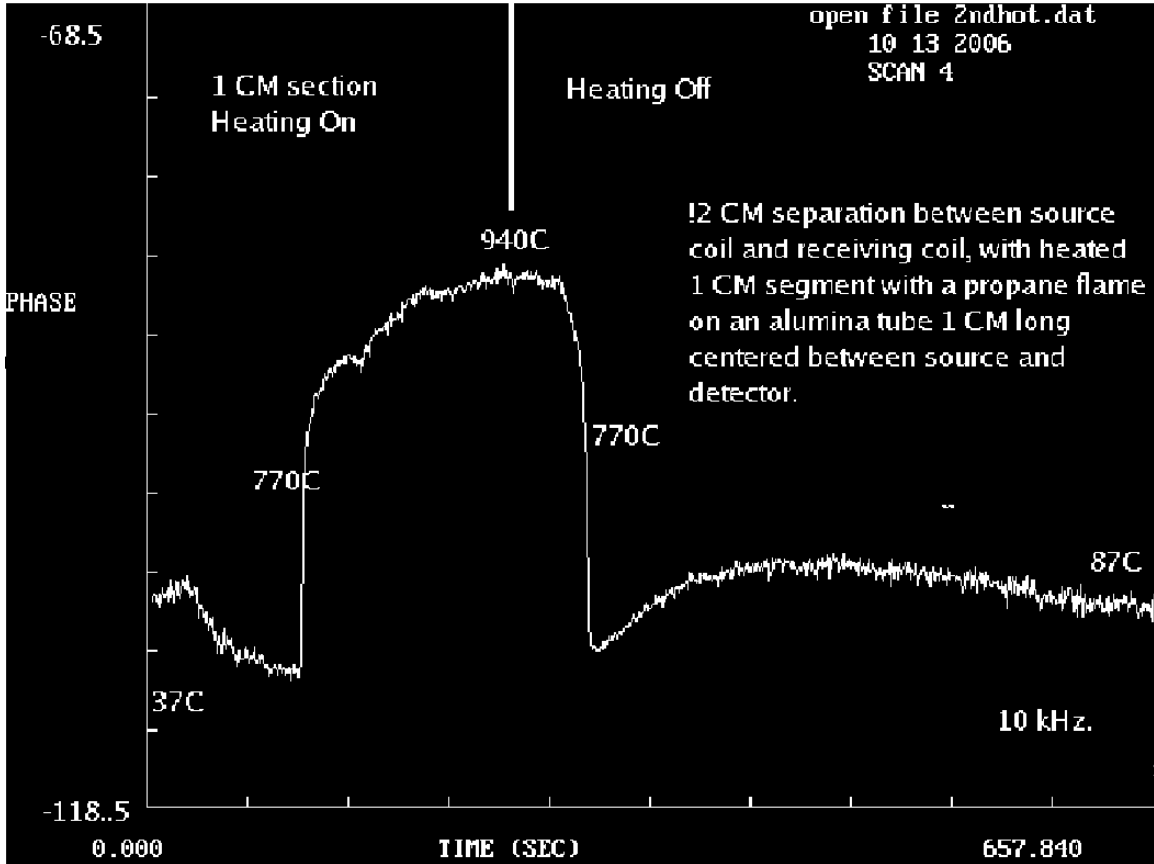


FIG. 7: The phase response of the 10 kHz transmission over 12 cm through a 1 cm hot zone in a 1018 steel rod. The sample starts at 37°C and is heated by flame to 940°C and allowed to cool to 87°C. The geometry is similar to figure 3b.

kHz	Phase Decrease	% Field Blocked	Gain to Curie Point	Comment
3	-24°	62%	131%	
5	-21°	43%	153%	
10	-31°	38%	271%	
20	-18°	16%	85%	
30	-8°	9%	38%	
50	-5°	4%	48%	
100	-4°	3%	1%	
200	-1.5°	> 1%	> 1%	
500	-1°	> 1%	> 1%	
1000	-.3°	> 1%	21%	on cooling
1850	-.7°	1%	6%	on cooling
2900	-.8°	2%	3%	on cooling

The heating for this particular data was done with a propane flame and not an electric furnace. If an electric furnace is used the results are much more complex depending on

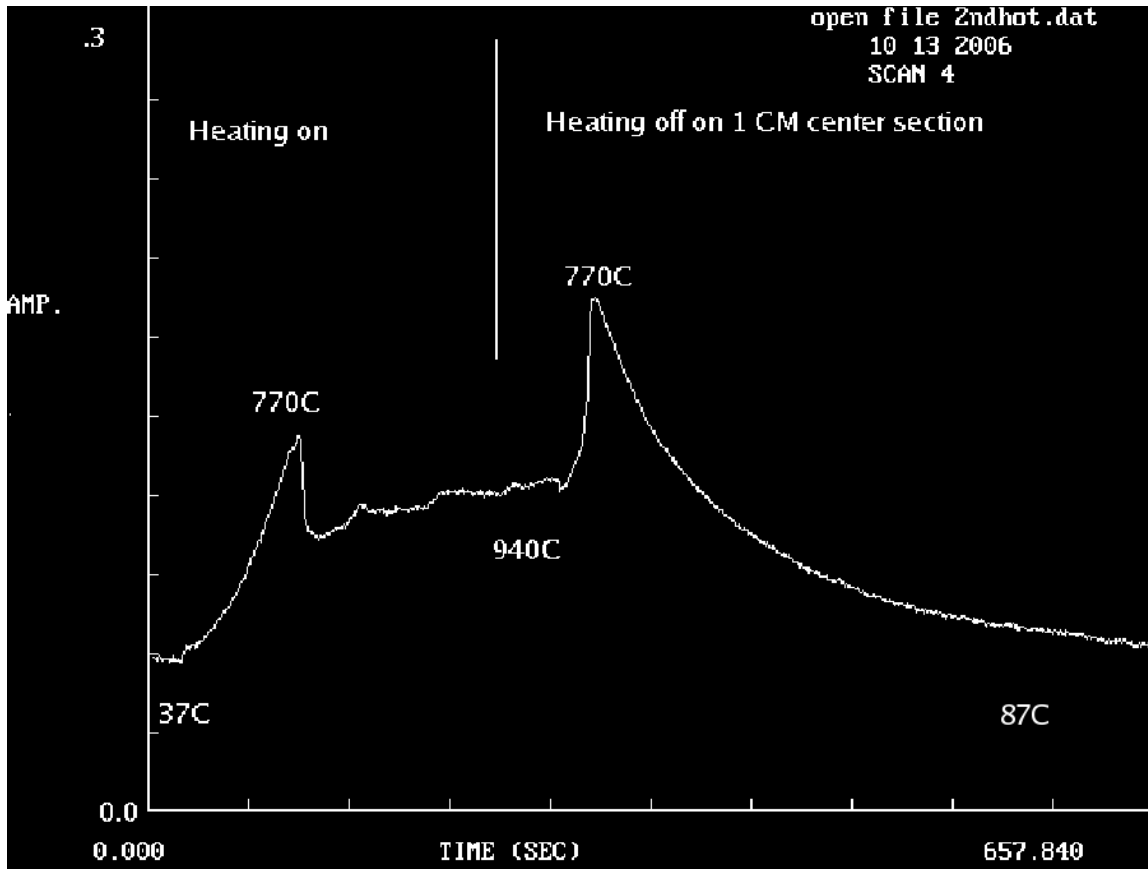


FIG. 8: The amplitude response of the 10 kHz transmission over 12 cm through a 1 cm hot zone in a 1018 steel rod. The sample starts at 37°C and is heated by flame to 940°C and allowed to cool 87°C. The geometry is similar to figure 3b and the source and receiver coils were cooled. The asymmetry in the response as the flame is removed represents the cumulative heating of the rod as heat diffuses outward from the center changing the gain characteristics.

the content of ripple in a DC supply or an AC power source is used because this induces a nonlinear interactions with the time varying heating field from the heating elements. If you were to replace the heat source with a local transverse strong static magnetic field at the center of the bar little change is measured.

Transmission and Dispersion Curves

The transmission measurement is a very useful experiment because if a resolvable field as a function of the source frequency can be identified with a measurable phase-distance relationship then a dispersion curve for that field can be constructed. Specifically this means that both the phase and amplitude data must be well behaved over a frequency range so that a field can be identified and enough points taken to reconstruct a dispersion curve. These measurements were taken in a 1018 hot rolled 12.7 mm diameter steel rod 69 cm long with the measurements done at 20°C. This material was selected because it is inexpensive and essentially well annealed iron with a low concentration of cementite precipitates, very

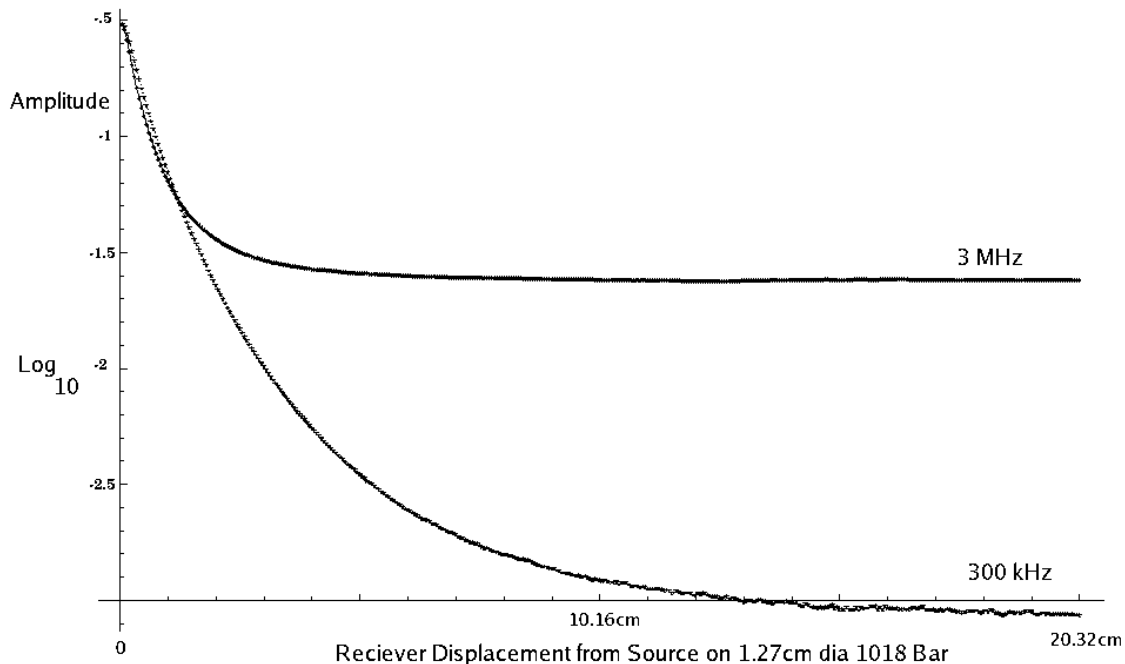


FIG. 9: Log_{10} Amplitude of a 300 kHz and 3 MHz signal verses separation from source. Displacement amplitude sample data above is one of a set of 15 scans at frequencies from 3 kHz to 3 MHz. The data was used to construct the transmission response graph in figure 11 along with the phase data for the same scan shown in figure 10.

little carbon in solution and annealed by the slow loss of residual heat stored in the large coil formed from a single billet after hot rolling. It suffers only a mild straightening operation with its *wüstite* patina in tack. Because of the heating and rolling in air and the visible oxidation there will be a surface decarburization band which will leave a relatively pure iron just below the oxide.

From the linear displacement of the receiving probe two well resolved fields were observed and one poorly resolved field with sample raw data from 2 of the 15 scan taken shown in figures 9 and 10. Field 1 below 30 kHz is possible an acoustical field driving a time dependent magnetization. This field is heavily damped with a detectable range of only 4 cm and estimated velocity of 4×10^3 m/s is shown in figure 11. This field 1 is only resolved at the lower frequencies and it could not be resolved above 30 kHz. The amplitude was difficult to separate from the source signal but it was significantly greater than 10 %.

The next dispersion curve is field 2 and it emerges resolvable from field 1 at 30 kHz. This field is detectable to 2 MHz, figures 11,13 and 14. This field's frequency has a parabolic dependence on the propagation vector consistent with the field carrier having a mass and behaving as a free particle. This field was not expected in a room temperature polycrystalline steel. This very low mass for field 2 makes it a candidate for a new type of quasi particle or a highly modified spin wave whose effective mass has been reduced. Above 2 MHz this field is not resolvable because its decay closely overlaps the source signal.

At higher frequencies beyond 500 kHz field 3 contribution grows, figure 14. This field is at the edge of being resolved at high frequencies because of its very small phase shift even though it has a large amplitude. In the Ln-Ln plot, figure 11, of the dispersion curve of field

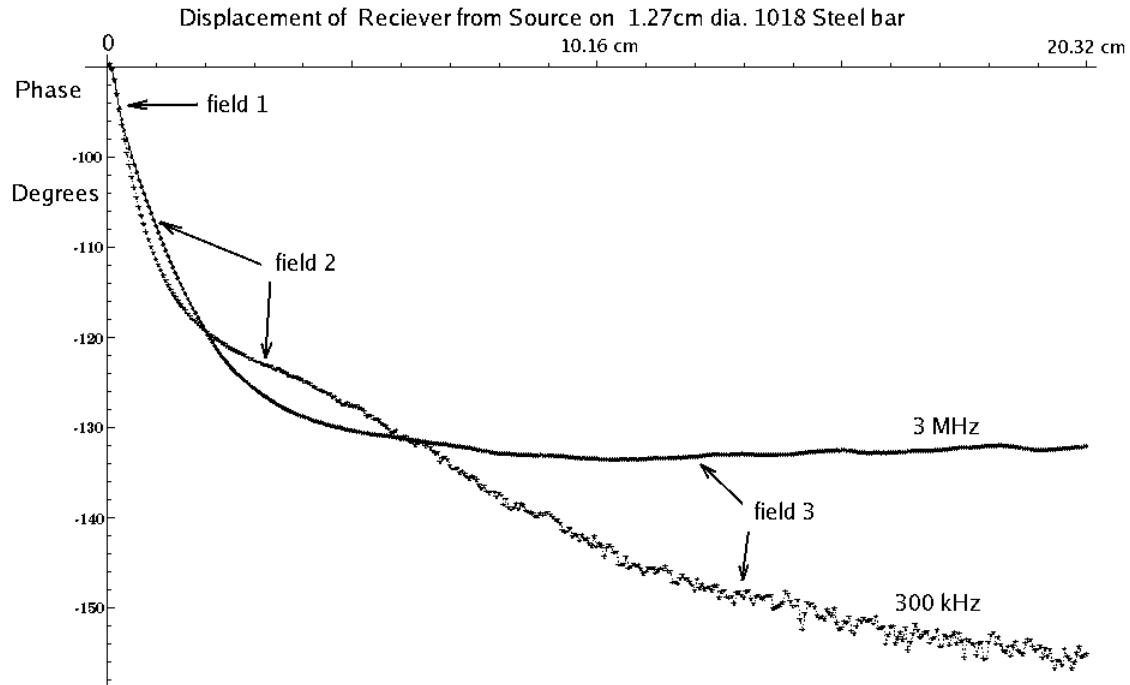


FIG. 10: Phase of a 300 kHz and 3 MHz signal verses separation from source in degrees. This is one of a set of scans from which phase data and displacement information was gathered. Data from these phase and amplitude scans were used to construct the three dispersion curves in figure 11.

3 it appears related to field 2 but as a mirror reflection. This implies that field 3 is really a measure of the density of a bound state rather than a propagating wave.

The behavior in the raw dispersion data of field 3 when amplified above 1.5 MHz is quite complex. These effects at 3 MHz are still small but they show both phase and amplitude modulation patterns that are indicative of new contributions from either the material or externally detected fields in combination with the source fields.

MECHANISMS AND SPECTRA

Source Field

In the transmission displacement scanning, the large signal detected near the source is assumed to be due to the contribution of propagating modes that have a radial components. These components are local to the source and their influence decreases rapidly as the sensor moves away from the source. But for those propagating modes that are rapidly attenuated their overlap with the source fields inhibits their extraction in this region near the drive.

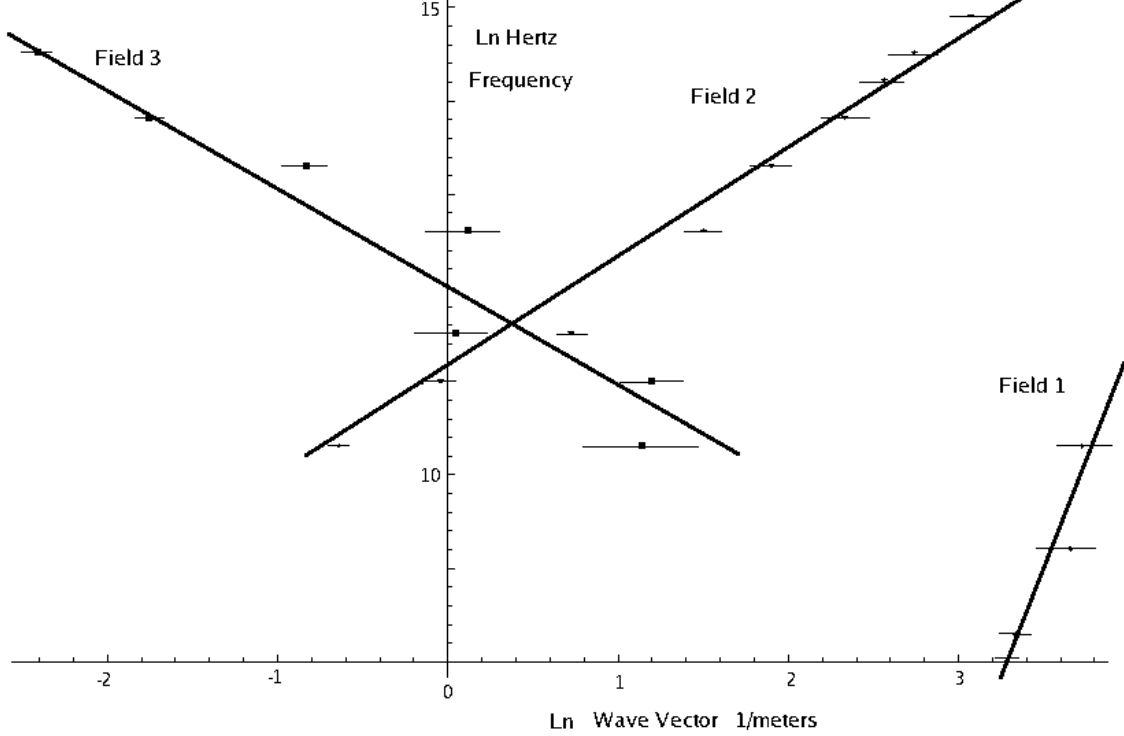


FIG. 11: To fit the three dispersion curves on a single graph a natural Ln-Ln plot in frequency for the vertical scale and propagation vector K in 1/meters. Field 1 has a velocity close to that of sound and is only seen below 30 kHz. Since the sensor is only sensitive to a time dependent magnetization, there would have to be coupling between fields. Field 2 has a computed effective mass of 1.8×10^{-39} kg ($1.3 \times 10^{-9} m_e$). Field 3 dominates above 500 kHz and rolls off very slowly. The intersection point of fields 2 and 3 provide for a degeneracy point where we could expect properties to be effected strongly.

Field 2

Of the three sections of dispersion curves found the more familiar but not necessarily trivial is that of field 2 and will be dealt with first. The zero field dispersion curve generated from neutron scattering(20) and all energies are in Joules and wave vectors are in $meters^{-1}$ for the thermal spin wave is:

$$E_{thermal} = 4.5 \times 10^{-40} \mathbf{q}^2 J \quad [10]$$

The dispersion curves extracted from figure 13 for the frequency range of 30 kHz. to 2 MHz. for field 2 is fitted to a simple quadratic function and yields:

$$E_{field2} = 4.69 \times 10^{-30} \mathbf{q}^2 J \quad [11]$$

The most impressive feature of the function is that its energy is scaled by a factor of almost 10^{10} greater than that of the thermal spin wave dispersion relation. This field is only detected unambiguously only in a window from 30 kHz to 2 MHz. Its amplitude increase with frequency as its range decreases. It has an effective mass of $1.8 \times 10^{-39} kg (1.3 \times 10^{-9} m_e)$.

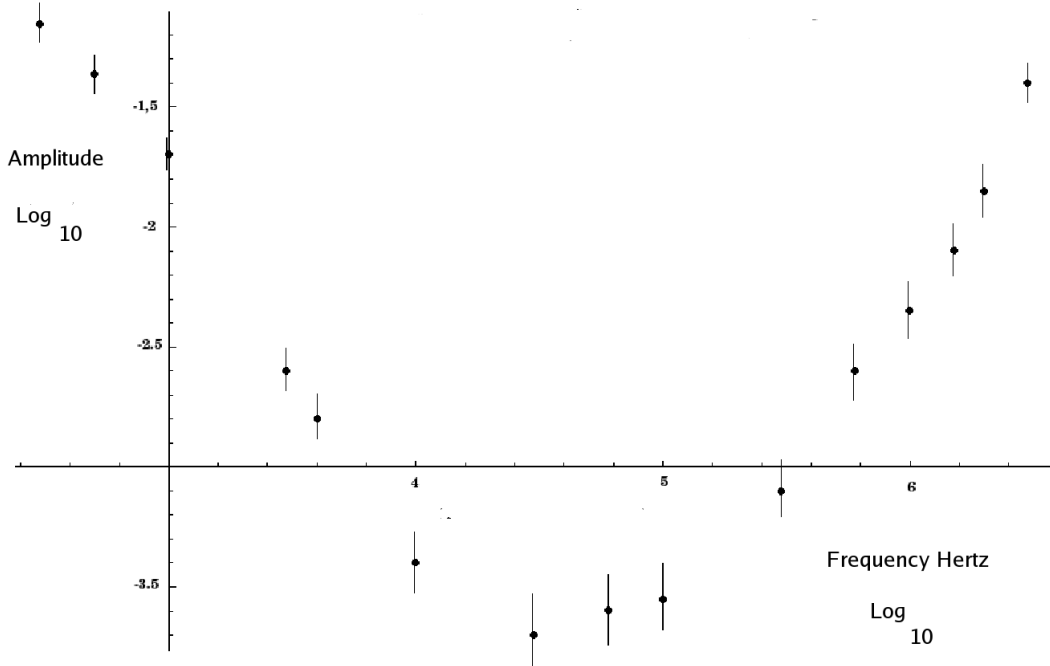


FIG. 12: Log_{10} Amplitude verse Log_{10} frequency for long range field at 20.32 cm from source. This data has a practical application in that for induction heating one would want to minimize the propagated energy loses and that would have a minimum for this particular steel between 10 and 30 kHz. This minimum is where induction heating of steel is found to be most efficient below the Curie point. This region also corresponds to the intersection of field 2 and 3. This degeneracy could lead to stronger scattering between these two states in addition to magneto-acoustic losses in this frequency window.

This is about 10 orders of magnitude greater than that of the thermal spin wave's effective mass. This very low mass for field 2 makes it a candidate for a new type of quasi particle or a highly modified spin wave whose effective mass has been reduced. The question is why associate this field with that of a spin wave. The first answer is that it is traveling measurable magnetization with a parabolic dispersion curve. The second answer is that the applied induction, $\mathbf{H}(\omega)$, will lift the phase degeneracy of the group of spin waves at the applied frequency via the contribution to the Hamiltonian, H_{int} .

$$H_{int} = -\mathbf{m}(t) \bullet \mathbf{B}(t) \quad [12]$$

This creates a single phase over a short distance that is favorably to collect a boson concentration. If this single phase condensation forms then the exchange scattering interaction of similar frequency spin waves to exchange phases ceases. This new allowed state will then have an effective mass determined by the scattering in its new state and its collective physical properties will be determine by its interactions. These effects in themselves are probably insufficient to produce such a large change in the wavelength or mass.

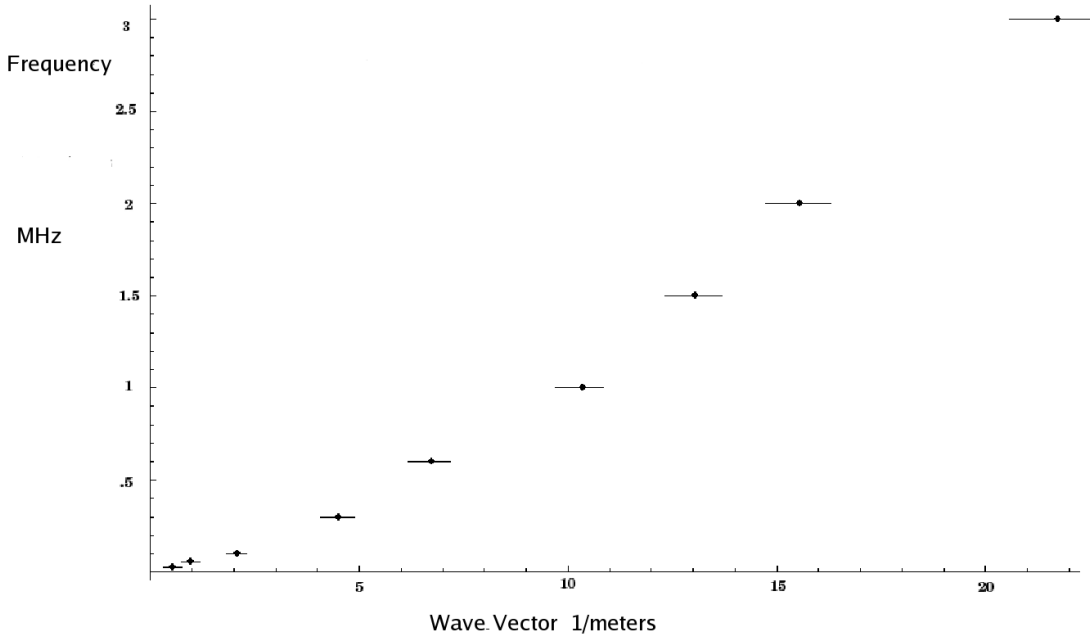


FIG. 13: **Field 2** plotted showing a parabolic relation between frequency and the propagation vector. This field was found to be resolvable in the range from 30 kHz to 3 MHz with both phase and amplitude data.

Field 1

Field 1 is the first initial sharp decrease in the dispersion measurements. This portion of the dispersion measurements represent a physical region within 2 to 3 cm of the source coil. This field is strongly damped and is short range. Above 30 kHz where the slope of the decrease was constant as a function of frequency this probably only reflects the fringing transverse fields from the source coil. But from 30 kHz downward a distinct dispersion curve can be extracted. The data for field 1 are not fit by a simple function that can be extended to zero frequency, if you take the local slope of the data to extract the velocity of the field values between 3600 and 5000 $\frac{\text{meters}}{\text{sec}}$, these numbers are not too different than acoustical velocities. There is a strong possibility that field 1 represents a coupled magneto-elastic wave(21) where a coherent long wavelength spin wave population can couple to stress wave. If we compute the phase velocity of field 2 we find that in the frequency range of 3 to 30 kHz. their values would run from 400 to 5000 $\frac{\text{meters}}{\text{sec}}$. This overlap in the velocities of field 2 with an acoustical wave velocity could allow a significant coupling to be established. The local dispersion curve for this coupled stress and spin wave field would be expected to be strongly varying as the spin wave velocity moved through and past the acoustical velocity. The wavelength of the field 1 excitation is between that of the thermal spin wave and the excitation of field 2. For example at 10 kHz. the wavelength of the field 1 is $\sim 25\text{cm}$ whereas the thermal spin wave is 60 microns and field 2's wavelength is on the order of 6 meters. The wavelength of field 1 is close to the acoustical wavelength at that frequency. The spin waves that form this coupled magneto-elastic wave are not from the thermal spin population but from the long wave length population of field 2.

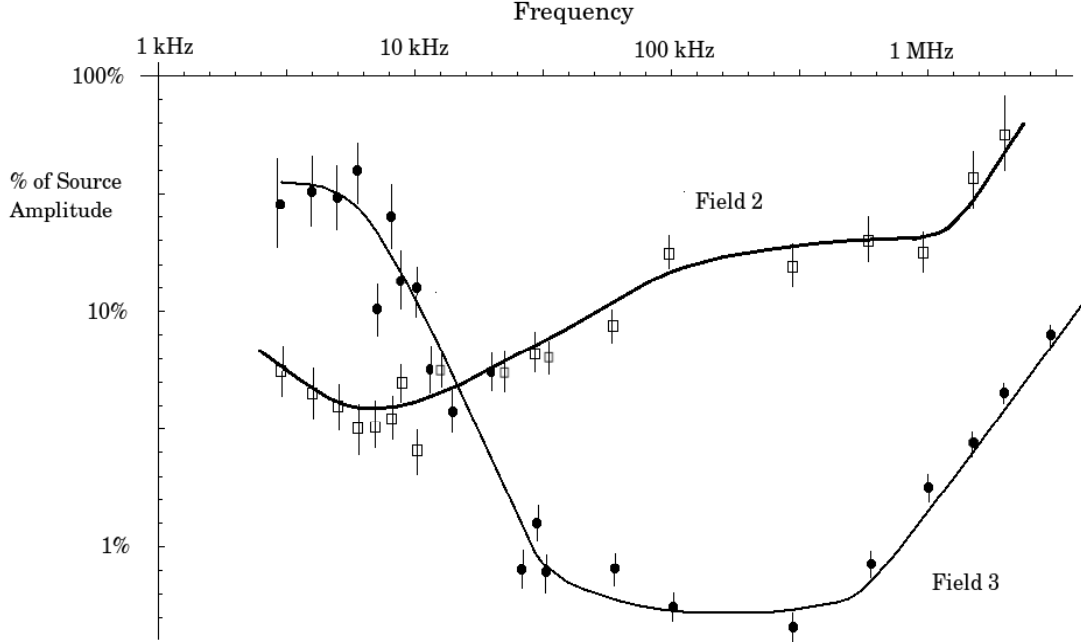


FIG. 14: From the amplitude displacement scans, the fields are extrapolated back to zero displacement to obtain the % of the source amplitude. The amplitude of field 1 is not plotted because it cannot be unambiguously separated from the source signal. Field 1, even though large at low frequencies, is a rapidly decaying short range field.

When the spin wave velocity of field 2 exceeds that of the speed of sound the stress and the spin wave fields should decouple. The velocity of field 2 is label v_2 and is computed below:

$$v_2 = \frac{1}{\hbar} \frac{\partial E_{field2}}{\partial q} = 8.89 \cdot 10^4 q \frac{m}{sec} \quad [13]$$

Using the experimentally fitted dispersion curve for field 2 and the speed of sound in iron at room temperature as $5130 \frac{m}{sec}$ we find that $q > .058 \frac{1}{m}$ this occurs at 30 kHz and it is precisely where field 2 can start to be unambiguously resolved.

Field 3

Field number 3 does not look like a traditional dispersion curve as it has the characteristics of a function describing a simple bound state. In a coarse examination it is approximately fit by a quadratic function to the inverse power of 2:

$$E_{field3} = \frac{1.15 \times 10^{-29}}{\mathbf{k}^2} J \quad [14]$$

This function looks qualitatively like a bound state function where k is proportional of n the principle quantum number. That indicates there is probably a significant interaction

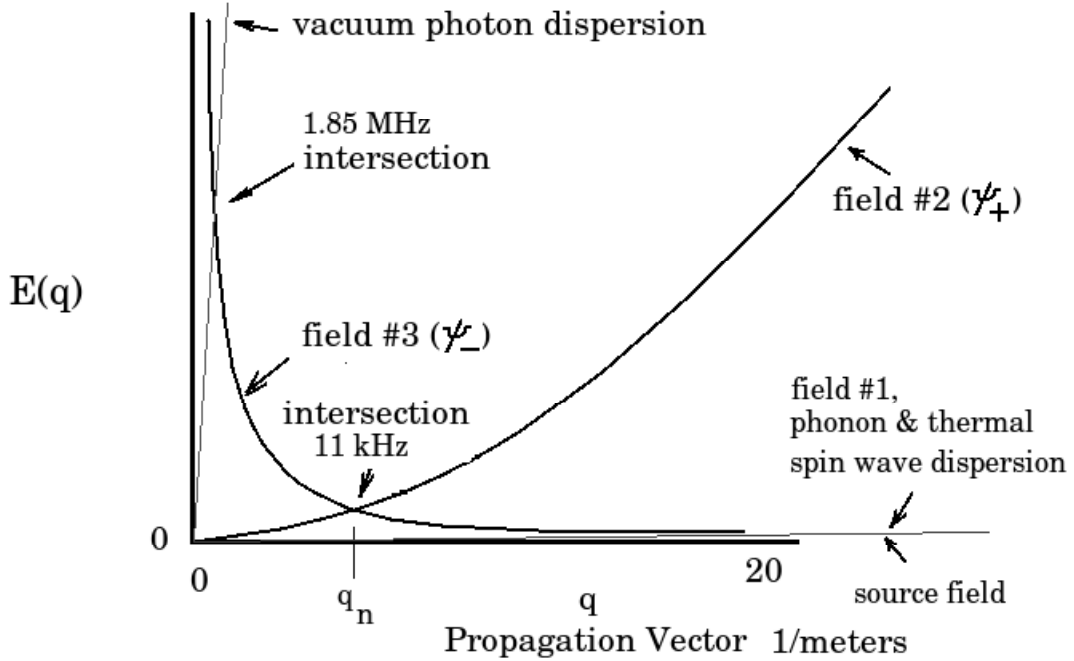


FIG. 15: Field 2 and field 3 are plotted with the vacuum photon dispersion curve. The intersection points are important as these are regions where energy can easily be exchanged between states. At frequencies greater 1.85 MHz the close proximity of the photon dispersion curve allows easy coupling between external fields and field 3. Intersection at 11 kHz, labeled q_n is associated with the minimum in transmission in figure 12 in the 10 to 30 kHz range. The two fields are degenerate at this crossing. The dispersion curves for field 1, internal transverse EM field, thermal phonon and thermal spin waves lie close along the $E \equiv 0$ axis at this scale of the propagation vector from 0 to $20 \frac{1}{meter}$. These fields provide a source for conserving momentum for transitions into or out of states of field 2, 3 and external radiation.

energy associated with excitations forming this state. This is particularly emphasized by the increased stability at higher energy as the size of the state grows larger. So for field 3 this is not a dispersion curve but a measure of the density of the state. The idea of bound spin wave states is not new and was introduced by Bethe(22) in 1931 for two spin waves on the same band with a net angular momentum of $J = 2$. The coupling there is a simple parallel spin-spin interaction term. That interaction does not look useful in this case. An interaction between two spin waves on different spin bands to produce a $J = 0$ state looks necessary. In addition, to having zero angular momentum the long wavelength state would weakly interact with the magnetic domain structure. The reason for considering the zero angular momentum boson is that its interaction are no longer strongly affected by magnetic domain orientations.

Placing the dispersion curves of fields 2 and density of field 3 in relation with other principle dispersion curves of the EM field in free space, thermal spin waves and thermal phonon can be seen in figure 15 which is a schematic representation of the key fields that will effect detected responses.

Populating a BELC with a Single Phase

High temperature Bose-Einstein like condensations (BELC) have been detected in spin wave systems that are laser pumped(23). The reason for differentiating this condensation from that of a BEC is that these are pumped at a frequency greater than zero. The expression for the transition temperature(25) to the BEC is :

$$T_{BEC} = \frac{\mathbf{n}^{2/3}}{m} \frac{2\pi\hbar^2}{k_b\zeta^{\frac{2}{3}}(\frac{3}{2})} \quad [15]$$

Where \mathbf{n} is the number of spin waves, m is the mass, ζ is the zeta function. To have a $T_{BEC} = 770^\circ\text{C}$ one only need an occupation number of greater than $\mathbf{n} = 5.78 \times 10^{12}$ and at 23°C the required density is 8.73×10^{11} .

To compare with the thermal spin wave density at 10 kHz one has density 6×10^8 at 23°C and 2×10^9 at 770°C . This indicates that forming BEC at either of these temperatures is only favorable if you pump the state with a non thermal source to form the state.

WAVE EQUATION FOR THE BELCS

The basic form of wave function for a BEC is the Gross-Pitaevskii equation(25) for the ensemble as a whole for a constant number of bosons is:

$$i\hbar \frac{\partial\psi(\vec{r})}{\partial t} = \left(-\frac{\hbar^2\nabla^2}{2m} + V(\vec{r}) + U_o|\psi(\vec{r})|^2\right)\psi(\vec{r}) \quad [16]$$

The induction problem considered here is a steady state problem where the number of spin waves is fixed by the drive amplitude. The sign of the potential U_o along with scattering determines the lifetime of the condensate. The solution of the equation with no external potential in the limit of low density reduces to the Schrödinger equation. Simplifying further assuming no binding potential to the matrix and the cyclical boundary value conditions are dropped the solutions then are not restricted to Block functions. The solutions can have wavelength greater than the sample size. By examining deviations in the band structure from free particle motion, $U_o(q)$ sign and magnitude could be extracted which contain the interaction of the elements in the BELC. In the limit of a low density population of BELC spin waves 10^{12} the term can be dropped for trial solution. The external potential, $V(\mathbf{r})$, has a value in the region of the source coil. The internal ferromagnetic magnetization $\mathbf{M}(x, y, z)$ is a rapidly varying function because of the domain structure and its integral over the volume of the sample will vanish as the size of the BELC structures are large relative to the MDBs. So that the Gross-Pitaevskii equation is just reduced to a free particle Schrödinger equation away from the the sources and picking a linear one dimensional geometry of figure 1, considering the solutions along the z-axis where the length of the bar is from $-\frac{L}{2}$ to $\frac{L}{2}$.

$$i\hbar \frac{\partial\psi(z)}{\partial t} = -\frac{\hbar^2\nabla^2}{2m}\psi(z) \quad [17]$$

This simple equation has solutions made up from the products $e^{\pm iqz}$, $e^{\pm az}$ multiplied by $e^{\pm i\omega t}$ where a is a real number. Taking the two positive energy solutions, the exponentially

decaying solution as ψ_- and the plane wave as ψ_+ . Our choice is helped from the experimental dispersion curves of figure 11. The parabolic curve looks very much like a simple free particle:

$$\psi_+(z, t) = \frac{1}{\sqrt{L}} e^{\pm iqz - i\omega t} \quad [18]$$

The hyperbolic dispersion curve for field 3 in figure 11 is even more interesting $E(k) \sim \frac{1}{k^2}$. This allows us to set $a = \frac{\alpha}{k}$ and then solution is a decaying exponential, where α has units of $\frac{1}{\text{meters}^2}$. This function describes a linear magnetic polarization of the medium coupled to the source which is not propagating. These are steady state responses and looks like an oscillating linearly polarized S state bound to the source.

$$\begin{aligned} \psi_-(z, t) &= \sqrt{\frac{\alpha}{k(1 - e^{-\frac{L\alpha}{k}})}} e^{-\frac{\alpha z}{k} + i\omega t}, z > 0 \\ \psi_-(z, t) &= \sqrt{\frac{\alpha}{k(1 - e^{-\frac{L\alpha}{k}})}} e^{\frac{\alpha z}{k} + i\omega t}, z < 0 \end{aligned} \quad [19]$$

The $\psi_-(z, t)$ state has a linear momentum $\langle p \rangle = 0$ unlike the propagating mode. This zero momentum solution is analogous to the zero momentum state of gas phase BEC. As the frequency is increased the size of the state is increases. This is a feature that dominates at higher frequencies. The two dispersion curves are

$$E_+(k) = \frac{\hbar^2 q^2}{2m} \quad [20]$$

$$E_-(k) = \frac{\hbar^2 \alpha^2}{2mk^2} \quad [21]$$

These two solutions are driven by the applied field are easily resolved in the frequency band 30 kHz. to 3mhz. The second solution has some interesting characteristic at high frequency the field decays very slowly spanning large distances relative to the source. The intersection point between the two dispersion curves only depends on the corrections to the effective mass as a function of their propagation vectors. The parameter α can be found from the crossing of the curves for field 2 and 3 from figure 11 at q_n then $\alpha = q_n^2$ assuming the effective mass of each state is the same.

The wave function has to be defined for the spin band on which the spin wave is moving. So that in the case of iron where there are two available bands the wave function would be in a vector form:

$$\psi_{\pm} = \begin{pmatrix} \psi_{\pm}^{\uparrow} \\ \psi_{\pm}^{\downarrow} \end{pmatrix}, \text{iron} \quad [22]$$

Originally the spin wave was proposed as an excitation to reduced the magnetization of the aligned ground state of a ferromagnetic material. For the right handed or left handed polarized spin wave on a single band the angular momentum was $J=1$ and it is opposed to the magnetization vector of the band. For a material with a net magnetization there is only one circular polarization active. This excitation has three components of time dependent magnetization $\mathbf{m} = (\theta, \theta + \frac{\pi}{2}, \theta + \pi)$ equivalent to the magnetic quantum number m . Since

within each magnetic domain there is a strong net moment only one circular polarization will be active on each band. This has its origins in the torque experienced by the band moments via $\dot{\mathbf{M}} = g\mathbf{M} \times \mathbf{H}$. For the spin up band this will be the right hand circular polarization ($\mathbf{RH}\uparrow$) and for the spin down band this the left hand circular polarization ($\mathbf{LH}\downarrow$). Within any magnetic domain these spin waves exist and interact strongly with magnetic domain boundaries (26). On a single band spin wave coupling of two spin waves will produce a higher angular momentum state, $J = 2$. With two available bands of opposite spin orientation, the coupling of two spin waves one on each band can produce a, $J = 0$, state with an axial time dependent magnetization. Considering the propagation vectors of the individual spin wave \mathbf{q} , the allowed orientation of two spin waves on opposite bands fall into the range $0 \leq |\mathbf{q}_{sum}| \leq 2|\mathbf{q}|$. In this range there are only two state that will be persistent. These are $\mathbf{q}_{sum} = 0$ and the $\mathbf{q}_{sum} = 2\mathbf{q}$. For other value of \mathbf{q}_{sum} the pair becomes non local and unbound. The $J = 0$ state is a very different in that across magnetic domain boundaries the strong force due a finite angular momentum with the changed spin alignments no longer operate. Also for this spin zero boson, the scattering between degenerate phase states is also removed as they don't exist for the spin zero pair. With the magnetic domain boundaries becoming transparent to the $J = 0$ states the change in physical properties of these coupled spin waves will be altered by operating across the entire sample.

Table 5: Pairing of spin waves on two bands where the total angular momentum is $J = 0$. The right hand($\mathbf{RH}\uparrow$) and left hand($\mathbf{LH}\downarrow$) polarizations are referenced to the orientation of the net local moment within a magnetic domain. The arrows refer to the specific band on which the spin wave is active. Because of a strong net moment only the $\mathbf{RH}\uparrow$ and the $\mathbf{LH}\downarrow$ polarizations are active on their specific bands. The value θ indicates the spin wave phase relative to the local applied time dependent field, and the orientation is the angle between the linear polarization of the magnetization and the axis of the time dependent field.

Band \uparrow and Phase	$\mathbf{RH}\uparrow \theta = 0^\circ$	$\mathbf{RH}\uparrow \theta = 0^\circ$	$\mathbf{RH}\uparrow \theta = 0^\circ$
Band \downarrow and Phase	$\mathbf{LH}\downarrow \theta = 0^\circ$	$\mathbf{LH}\downarrow \theta = \pi$	$\mathbf{LH}\downarrow \theta = \frac{\pi}{2}$
Polarization	Linear	Linear	Linear
Orientation	0°	$\frac{\pi}{2}$	$\frac{\pi}{4}$

The only phase that is energetically favorable with respect to a time dependent source field is the first column where both the left and right hand components are in phase with the applied field. The second column is also worth noting that if the phase of one component is shifted by π during an interaction then the orientation of the magnetization rotates by $\frac{\pi}{2}$ which is an easy condition to detect.

There are really two regions where the time dependent vector potentials needs to be consider. First is the region under the source coil and second in the remainder of the bar. These fields are very different. The induced source field is a rapidly decaying transverse field limited to the material near surface directly under the inductor. The field due to the long wave length spin waves is a very slowly spatially varying field. The wave length of the magnetization signals are long relative to thermal spin waves, the source appears almost as a delta function source at the location of the coil. This source function is given by the interaction Hamiltonian, H_{int} , which is the product of the applied field with the time dependent magnetization. Away from the source the time dependent magnetization of

the BELC provides a field energy that is dependent on the interaction between the created BELC components. Because the curl of this BELC driven field is small, eddy current losses will be small. An example of these fields slowly varying distributions probed with a small sensor over a larger bar than can be found in reference (27) where a field produced from BELC interactions generate a uniform field across the bar away from the source.

The two fields isolated above 30 kHz represent a propagating mode, ψ_+ which has a real momentum and a bound state, ψ_- with zero net momentum. The transmission experiment where the center of the bar was raised above the Curie point, shows a drop in transmission with an abrupt decrease in phase delay. From the dispersion relations at frequencies greater than 1 kHz the phase delay at a fixed offset is less for ψ_- than for ψ_+ . Considering this phase property, ψ_+ looks filtered or reflected out and ψ_- has managed to penetrate this paramagnetic region without significant attenuation.

Coupling Spin Waves to Form $J = 0$ Pair

The wave equation solution for the spin wave excitation, ψ_+ is a good representation for the measured field 2 of figure 11. However field 3 is represented by, ψ_- is a decaying spin wave state that dominates at high frequencies and appears to be able to traverse regions above the Curie point. The question is what can drive the formation of a $J = 0$ state which is quite unlike the $J = 2$ coupled state for spin waves on the same band. These long wavelength excitations are measured a sample of finite size much smaller than their wavelength. In an isotropic material one can calculate the magnetic field energy of two separate configurations bound or separated spin waves where the symmetries and phases are matched to produce an axial magnetization of the paired state as defined in the previous section.

$$H_{separate} = (0, \cos(\omega t)H_1, \sin(\omega t)H_1) \times 2 \quad [23]$$

$$H_{pair} = (0, 0, 2\sin(\omega t)H_1) \quad [24]$$

computing the squares of the field and multiplying by the vacuum permeability, μ_0 .

$$E_{separate} = -\mu_0 H_1^2 \quad [25]$$

$$E_{pair} = -\frac{\mu_0}{2} \langle 4\sin^2(\omega t)H_1^2 \rangle = -\mu_0 H_1^2 \quad [26]$$

The field energies for the two configurations are identical and there is no driving force for forming a bound pair. The calculation for strain energy due to the spin wave field is similar showing equal contribution to both configurations. However, iron based alloys are magnetically anisotropic with $\sim 30\%$ increase in the permeability(28) along the easy magnetization cube axis, $\langle 100 \rangle$. The orientation dependent strain energy contribution is going to be neglected. The bulk of the spin waves energy lies in its magnetic field this anisotropy gives a reduction in energy for the linearly polarized magnetization on the easy axis of $\sim -\frac{\hbar\omega}{3}$, which is a large interaction energy favoring the formation of coupled spin wave pairs. So that texture and grain orientation can play a large role in the ability to form the paired state BELC. To calculate the effect of the anisotropy on the binding energy, the random orientation of a collection of grains with projections on the easy axis and the hard

axis have to be made on a line. For any line segment taking a random selection of the three orientations, $\frac{1}{3}$ falls on an easy axis. This occurs for both the paired and separate states so there is no driving for binding a paired state. However, if the hot rolled textures the bar tested was preferentially $\langle 100 \rangle$ along the long axis then the paired states would be preferential. Orientation texture comes from two source, the original as cast grain orientation columnar growth into the melt is typically $\langle 100 \rangle$. In continuous cast product this is not the case for the entire billet cross section. The casting growth proceeds from the wall of the casting and from the bottom in the middle portion of the casting so that the cast texture is mixed. The second source is from secondary recrystallization after cold rolling and this is tied to minimizing surface energy of a sheet which is not the case for this bar. Oriented single crystal of iron, and cold rolled sheet should show these effects but not hot rolled rod.

The mechanism that is active in driving the binding of spin pairs in poly crystalline material arises from the minimization of leakage field at the surface. The energy of the bound state will be decreased because the fields normal to surface of the material will vanish. The leakage fields contribute to this higher energy for the unpaired spins can be seen by replacing μ_o with μ for the \mathbf{z} component of the field in the limit of a very thin rod when $\mu > \mu_o$.

$$E_{separate} = -\frac{\mu + \mu_o}{2} H_1^2 \quad [27]$$

$$E_{pair} = -\frac{\mu}{2} \langle 4 \sin^2(\omega t) H_1^2 \rangle = -\mu H_1^2 \quad [28]$$

$$E_{pair} < E_{separate} \quad [29]$$

This rough calculation is valid when $\mu > \mu_o$ for the energetics of the $J = 0$ paired states as compared to two separately located spin waves making pairing favorable at all frequencies when driven with a time dependent field. This would be true for either the non propagating ψ_- or the propagating ψ_+ field. This argument can be generalize for an inhomogeneous material which contains magnetic domain boundaries, secondary phases such as oxides, martensite, austenite, carbides or hydrides. Writing the permeability as:

$$\mu_{ij} = \frac{\partial B_i}{\partial H_j} = \sum_k \frac{\partial B_i}{\partial x_k} \frac{\partial x_k}{\partial H_j} \quad [30]$$

Considering those regions where \mathbf{H} is slowly varying and $\frac{\partial x_k}{\partial H_j} \neq 0$. The quantity $\frac{\partial B_i}{\partial x_k}$ carries the measure of the inhomogeneity in the permeability. It is this quantity that reflects $\mu_{ij}(\mathbf{x}, \omega)$ variation in the material. If $\mu_{ij}(\mathbf{x}, \omega)$ is not a constant function over the material then there will be an energetically favorably coupling between spin waves to form axial magnetization pair with $J = 0$ if the band structure allows such a state. The strength of the coupling will depend on the integral of $\frac{\partial B_i}{\partial x_k}$ over the volume which can take on large values traversing the magnetic domain boundaries and second phase precipitates.

Reversing the picture again and having ferromagnetic precipitates in a non ferromagnetic matrix is much like the first simple model presented above. Some non magnetic matrix that have embedded ferromagnetic material seem to be able to support the linear time dependent magnetization of these bound spin wave fields with minimal loss. This becomes important in the non destructive testing of stainless steel welds by inductive techniques where the heat affected zones and the weld zones contain a small minority of ferromagnetic precipitates whose responses can often mask large physical defects.

Coupled Spin Waves Interactions and BELC Stability

One feature of a stable BEC is that the particles involved should show a repulsive interaction if the state is to be easily formed. This interaction can be computed from the density variation as one considers the displacement of two particles by an amount Λ . There are three different cases of interest. The first two are inter particle interaction between states of the same type. The third case is the interaction between a displaced ψ_+ and a ψ_- state. In the case of large sample size relative to the wave length the plane wave solution ψ_+ produces no net interaction. However, in truncated sample the net interactions are altered. If the wave length is long then one can take a trial function $\psi_+ = e^{i(\mathbf{q}\mathbf{x}-\omega t)}$. The wave functions of equation 18 and 19 can be expanded for the near field behavior as the bar length, L , is a highly truncated space:

$$\psi_+ \approx \frac{1}{\sqrt{L}} e^{-i\omega t} (1 + i\mathbf{q}\mathbf{x}) \quad [31]$$

Similarly this can be done for the ψ_- in the case of state that is larger compared to the bar length:

$$\psi_- \approx \frac{1}{\sqrt{L}} e^{+i\omega t} \left(1 - \frac{\alpha x}{k}\right) \quad [32]$$

Now the time dependent magnetization must be added to the system for the two bands and it has to absorb the time dependency explicitly.

$$\psi_{\pm} \approx f(\mathbf{x}, \mathbf{q})(\mathbf{M}^{\uparrow}(t) + \mathbf{M}^{\downarrow}(t)) \quad [33]$$

Where for a spin one boson the magnetization for one band are represented by three states relative to the phase of the local source field θ and the bold face state is in phase with the source field within the sample and in the coupled coherent state on the in phase spin wave field component remains:

$$\mathbf{M}(t, \theta) = \begin{pmatrix} \mathbf{m}(t, \theta) \\ m(t, \theta + \frac{\pi}{2}) \\ m(t, \theta + \pi) \end{pmatrix} = \begin{pmatrix} \mathbf{m}(t, \theta) \\ 0 \\ 0 \end{pmatrix} \quad [34]$$

$$\begin{pmatrix} \mathbf{m}^{\uparrow}(t, \theta) \\ 0 \\ 0 \end{pmatrix} + \begin{pmatrix} \mathbf{m}^{\downarrow}(t, \theta) \\ 0 \\ 0 \end{pmatrix} \Rightarrow (\mathbf{m}^{\uparrow}(t, \theta) + \mathbf{m}^{\downarrow}(t, \theta)) \quad [35]$$

The $J = 0$ paired function ψ_+ and ψ_- become:

$$\psi_+ \approx \frac{1}{\sqrt{L}} (1 + i\mathbf{q}\mathbf{x})(\mathbf{m}^{\uparrow}(t, \theta) + \mathbf{m}^{\downarrow}(t, \theta)) \quad [36]$$

$$\psi_- \approx \frac{1}{\sqrt{L}} \left(1 - \frac{\alpha x}{k}\right) (\mathbf{m}^{\uparrow}(t, \theta) + \mathbf{m}^{\downarrow}(t, \theta)) \quad [37]$$

It is possible that the large effective mass of the thermal spin wave has its origin in the interaction of the six $\mathbf{m}^{\uparrow\downarrow}(\theta)$ states with each other that are populated in addition to the magnetic domain boundaries. If there were higher angular momentum states with coupling

on the same band at the same wave vector the number of interacting states would increase. The $J = 0$ states allow the functions to span the magnetic domain boundaries and removes the scattering into other degenerate phase states which no longer exist.

Two Particle Interactions

Now there is simple calculation that can be done on both wave functions to determine the sign of the inter particle potential interaction if the one wave functions is displaced a distance , Λ . The bar is a truncated space on which a set of slowly varying wave function are considered. Using the data in figure 1 that the potential will be a minimum for the higher density of coherently coupled spin waves. This makes the sign negative on the integrals for a density increase over the bar to scale an interaction energy.

$$\delta\rho_{++}(\Lambda) \sim \frac{1}{L} \int_{-\frac{L}{2}}^{\frac{L}{2}} (\psi_+^*(0) + \psi_+^*(\Lambda))(\psi_+(0) + \psi_+(\Lambda))dx \quad [38]$$

$$\psi_+(\Lambda) = \frac{1}{\sqrt{L}}(1 + iq(x - \Lambda)) \quad [39]$$

Just taking the term with a factor of the separation Λ where:

$$\delta\rho_{++}(\Lambda) \sim q^2\Lambda^2 \quad [40]$$

The potential as a function of Λ is proportional to the negative of this density :

$$V_{++}(\Lambda) \sim -q^2\Lambda^2 \quad [41]$$

The inter particle interaction is repulsive and increasing in strength with frequency for this excitation.

For the case of the ψ_- excitation the resulting integral has to be done over three ranges of over lapping functions:

$$\delta\rho_{--}(\Lambda) \sim \frac{1}{L} \int_{-\frac{L}{2}}^{\frac{L}{2}} (\psi_-^*(0) + \psi_-^*(\Lambda))(\psi_-(0) + \psi_-(\Lambda))dx \quad [42]$$

Where

$$\begin{aligned} \psi_-(\Lambda) &= \frac{1}{\sqrt{L}}(1 - a(x - \Lambda)), x > \Lambda \\ \psi_-(\Lambda) &= \frac{1}{\sqrt{L}}(1 + a(x - \Lambda)), x < \Lambda \end{aligned} \quad [43]$$

computed over the three regions of overlap the result is:

$$\delta\rho_{--}(\Lambda) \sim a^2\Lambda^2 + 4a\Lambda\frac{\Lambda}{L}\left(1 - \frac{a\Lambda}{3}\right) \quad [44]$$

This results in a potential dependent on the separation Λ which is interesting in that it can be both attractive and repulsive depending on the length of the sample and the frequency.

$$V_{--}(\Lambda) \sim -a^2\Lambda^2 - 4a\Lambda\frac{\Lambda}{L}\left(1 - \frac{a\Lambda}{3}\right) \quad [45]$$

The interaction cannot be attractive unless:

$$\frac{a\Lambda}{3} > 1 \quad [46]$$

which can only occur at high frequencies.

The third interaction is that between ψ_- and ψ_+ and that can be computed with the integral:

$$\delta\rho_{+-}(\Lambda) \sim \frac{1}{L} \int_{-\frac{L}{2}}^{\frac{L}{2}} (\psi_+^*(0) + \psi_-^*(\Lambda))(\psi_+(0) + \psi_-(\Lambda))dx \quad [47]$$

The resulting density dependence on the separation is:

$$\delta\rho_{+-}(\Lambda) \sim a^2\Lambda^2\left(1 - \frac{4}{aL}\right) \quad [48]$$

This interaction can only go attractive at low frequency when $\frac{4}{aL} > 1$ or if the sample size is small.

SPECTROSCOPY OF THE BELC AND INDUCTION ANALYSIS

The kinetics of pumping BELCs are controlled by the density of mobile magnetic domain boundaries. At the magnetic domain boundaries the magnetization transitions through zero allowing the applied source fields to drive transitions. The principal transition will be to drive the ground state, aligned ferromagnetic ordering, into a time dependent state. The applied field will couple the vacuum state into ψ_+ or ψ_- .

The fundamental difference between a BELC and a BEC is the time dependence associated with the BELC and it has to be continuously pumped as a steady state process at a finite frequency $\omega > 0$. The easiest way to explore this is with a perturbation. These states are not easily perturbed, there are few structures that alter their characteristics. The simplest measurable perturbation is to induce a second perturbing BELC where we can alter its level. Going back to figure 3b of our transmission experiment and changing the geometry slightly by replacing the heat injected into the center of the bar with a low frequency field time dependent field $\mathbf{H}(\omega_2 t)$. A coil of the same type will be used to inject the center field. By displacing the two fields by a 5 centimeters we are insuring that we do not have a direct superposition of our two applied fields.

Our original field injected at the end will be ω_1 driven at the same levels $\mathbf{H}(\omega_1 t)$ as our transmission experiments. The fields are driven under these conditions, $\omega_2 \ll \omega_1$ and $|H(\omega_2)| > |H(\omega_1)|$. The spacing separation between the source and the receiver is set at 10 cm. As the field level $H(\omega_2)$ is increased two states emerge, the strongest being $|\omega_1 - 2\omega_2 >$ followed by $|\omega_1 + 2\omega_2 >$ and if the field level is increased a little more another pair of states develop with the strongest being $|\omega_1 + \omega_2 >$ followed by $|\omega_1 - \omega_2 >$. At this stage the original probe field $|\omega_1 >$ has managed a gain in amplitude of about 4%. A spectra of these are shown in figure 16.

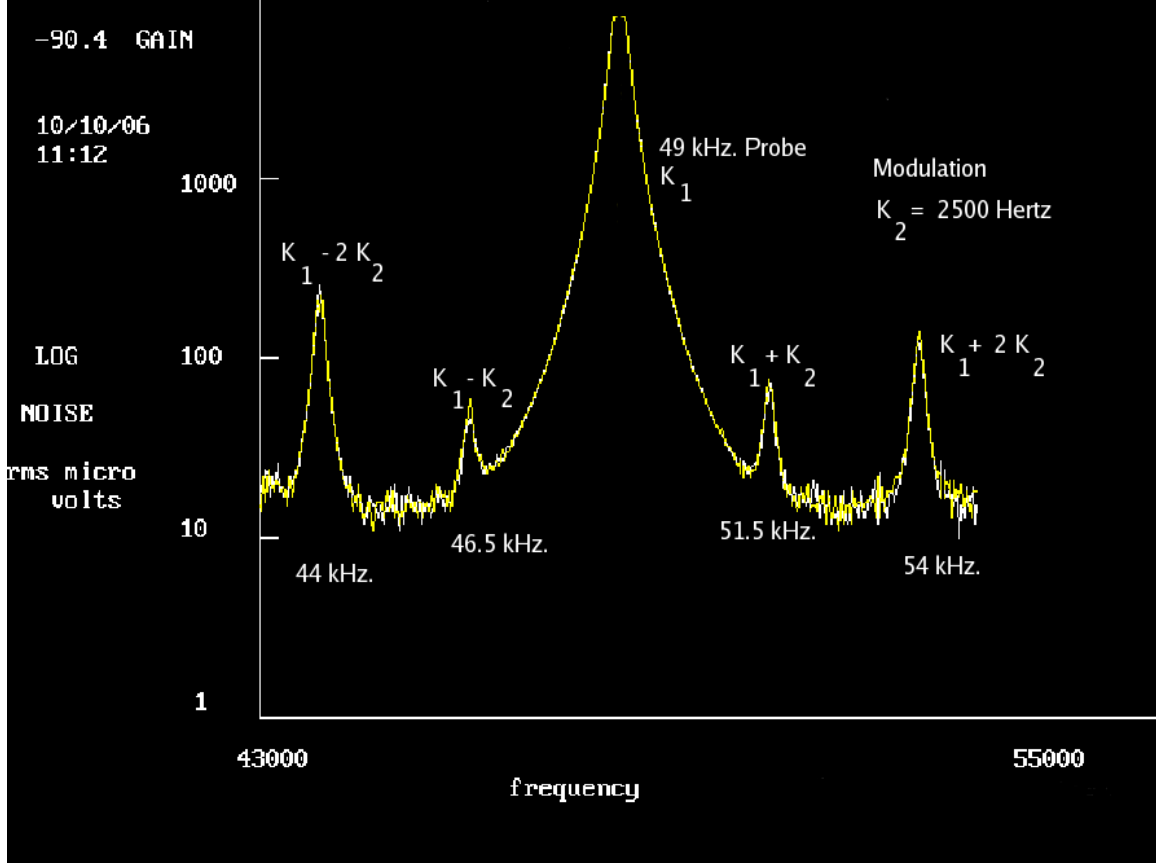


FIG. 16: The 4 principal transitions observed when two BELCs overlap. K_1 is the wave vector for the weaker probe field ω_1 and K_2 is the wave vector for the stronger drive field ω_2 injected at the center of the bar. All signals are detected at the opposite end of the bar that is 10 cm away.

If you keep increasing the drive level of ω_2 you generate a spectral comb of states $|\omega_1 \pm n\omega_2\rangle$ where n is an integer. The even number states and odd number states differ in how the transitions alter the polarization of the magnetization relative to the propagation vector so that apparent strengths of transitions are dependent on the geometry and the interaction that are active when measured. There are other measurement geometries more suited to working out the details of the individual transitions. The full set of coupling from table 6 need to be considered as possible contributors to this spectra.

There is a possible fault in this view of the spectra. In figure 4 the single coil response shows a marked nonlinear behavior for iron and because of this one would expect to generate the product and difference fields when two fields are superimposed on the material. In this case the introduced fields are physically displaced as is the detector. Second the spectra generated are more characteristic of linear and angular momentum conserving reactions forming their own BELC as they are then found at a remote detector. Simply having a local nonlinear field response does not account for their migration to the detector or the details of the spectra.

Table 6: Relative transition strengths with a probe field ω_1 of 49 kHz. The strengths are taken at the extrapolated limit for the injected field $\omega_2 \rightarrow 0$.

Transition	Strength = % of $\langle \omega_1 \omega_1 \rangle$
$\langle \omega_1 V_1 \omega_2 \rangle$	$4 \pm .1$
$\langle \omega_1 - 2\omega_2 V_2 \omega_1 \rangle$	$2.4 \pm .1$
$\langle \omega_1 + 2\omega_2 V_2 \omega_1 \rangle$	$1.4 \pm .1$
$\langle \omega_1 + \omega_2 V_3 \omega_1 \rangle$	$.9 \pm .1$
$\langle \omega_1 - \omega_2 V_3 \omega_1 \rangle$	$.8 \pm .1$

Hamiltonian for the Transitions

The kinetic portion of the Hamiltonian for the propagating spin wave excitation neglecting their mutual and external field interactions can be written as a free particle is :

$$H = \frac{1}{2m_{s-w}} \sum_j \hbar^2 \mathbf{q}_j^2 \quad [49]$$

In a material like iron where the conduction electrons are also participating in the spin wave excitation the Hamiltonian will include the kinetic terms for the electron. The electrons in turn are acted upon by any field present. The effect of the slowly varying vector potential which is only due to the BELC's themselves should be a break on the momentum(29) where $\mathbf{p} \rightarrow \mathbf{p} - \frac{e}{c} \mathbf{A}$. Since the conduction electrons supporting the spin waves are acted on by the same field the momentum of the spin waves will also be altered by the external vector potential. Therefore the same transformation, $\hbar \mathbf{q} \rightarrow \hbar \mathbf{q} - \frac{e}{c} \mathbf{A}$, for the field dependent momentum has to be made for a material like iron. The total wave function which will include the spin wave contribution will act on the two field dependent terms of the vector potential. The velocity of the fields within the conductor will not be speed of light in vacuum but will be the phase velocity of the particular component of the vector potential that is being considered. The induced transverse field will have a substantially reduced phase velocity equal to $\sqrt{\frac{\omega}{\mu\sigma}}$. This will also amplify transitions driven by these fields.

$$H = \frac{1}{2m_{s-w}} \sum_j (\hbar \mathbf{q}_j - \frac{e}{c} \mathbf{A})^2 \quad [50]$$

With the mass of the electron so much greater than that of the BELC spin wave the two field dependent terms in the spin wave portion of the kinetic energy get amplified in their ability to drive transitions by a factor of 10^9 .

The vector potential \mathbf{A} is actually considered in two parts, that of the source field, \mathbf{A}_{ext} and the vector potential due to a specific BELC field \mathbf{A}_i . The external field, \mathbf{A}_{ext} , is a locally acting field and \mathbf{A}_i acts over the entire volume. They arise from

$$\mathbf{B} = \mu_o \mathbf{H}_{ext} + \sum_i^{BELCs} \mathbf{M}_i = \nabla \times \mathbf{A} \quad [51]$$

where

$$\nabla \times \mathbf{A}_i = \mathbf{M}_i \quad [52]$$

$$\mathbf{A} = \mathbf{A}_{ext} + \sum_i^{BELCs} \mathbf{A}_i \quad [53]$$

These two fields have very different spatial distributions. In the computation of the induced vector potential field \mathbf{A}_{ext} at the source within a homogenous conductor the solution is a single, inward propagating, exponentially decaying field. This correct solution actually disguises what is taking place. There are in fact two field $\vec{\mathbf{A}}$ and $\overleftarrow{\mathbf{A}}$ along with circumferential current \mathbf{j}_θ . One field propagating inward $\vec{\mathbf{A}}$ and a reflected field $\overleftarrow{\mathbf{A}}$. The quadratic then becomes:

$$\mathbf{A}_{ext}^2 = \vec{\mathbf{A}}^2 + \overleftarrow{\mathbf{A}}^2 + 2\vec{\mathbf{A}}\overleftarrow{\mathbf{A}} \quad [54]$$

The third term is the interesting term in that it carries no linear momentum. A two photon absorption into the vacuum state can produce a pair of spin waves with net zero linear momentum while conserving angular momentum and energy for a two spin wave transition. This break down of the vector potential only occurs in conductors. The reflection response in nonconducting ferrites are in phase with the source fields and the term is simply \mathbf{A}^2 . This a consideration for conductors alone.

With vector potentials in the range of 10^{-5} to 10^{-10} tesla meter for the range of experiments the strength of the transitions depends very much on the magnitude of \mathbf{A} .

Table 7: Comparison of transition strengths, m_e electron mass and c is the speed of light in vacuum, set q for spin wave = 1. The velocity of light in the metal is that of a transverse electromagnetic field at 10 kHz. This velocity is closer to the speed of sound that the speed of light in vacuum.

mass	velocity	q	$\frac{2e\hbar q}{mc} \mathbf{A}$	$\frac{e^2}{mc^2} \mathbf{A}^2$
m_e	c	1	$10^{-31} \mathbf{A}$	$10^{-25} \mathbf{A}^2$
mass spin wave $10^{-9}m_e$	c	1	$10^{-22} \mathbf{A}$	$10^{-16} \mathbf{A}^2$
mass spin wave $10^{-9}m_e$	$\sqrt{\frac{\omega}{\mu\sigma}} \sim 10^{-5}c$	1	$10^{-17} \mathbf{A}$	$10^{-11} \mathbf{A}^2$

The role the reduced effective mass of the spin wave plays in allowing transition due to the vector potential to the first or second power is large. The further enhancement by considering the reduce velocity of light within the metal to drive transitions from the source current is also significant compared to the coupling to a free electron. The next feature that plays a large role in the interaction of the BELC is that their field is slowly varying over the bar and the effective vector potential for the same \mathbf{B} level is greater by the ratio of the source penetration depth to the diameter of the rod. This further enhancement by a factor of 10 to 100 for the BELC field to drive transitions will promote interactions between BELCs. At field levels for the vector potential at 10^{-5} Tesla-meter the linear and quadratic terms in the Hamiltonian approach each other in value. This would then be expected to allow the two types of transition of the kind found when energy, linear and angular momentum are conserved.

Now we can consider the transitions that are allowed between the spin waves and the applied field solely. This is summarized in the following table. The conditions are that linear

momentum and angular momentum must be conserved along with energy and the phase of the interactions are assumed to be preserved. The first transition to consider is that from the ground state. The controlling element is the small linear momentum associated with a photon $\frac{\hbar\omega}{c}$ compared to that of the propagating spin wave mode.

Table 8: Transition for the Linear Geometry

Transition	final state	ΔJ
$\langle +q, \omega; -q, \omega \mathbf{A}(\omega)^2 0 \rangle$	$ 0 \rangle \Rightarrow \psi_-$; allowed, direct to a paired state	0
$\langle q, \omega \mathbf{A}(\omega) 0 \rangle$	\mathbf{p} not conserved without phonon or other, not a pair process	1
$\langle \omega_1 \pm \omega_2 \mathbf{A}(\omega_2) \omega_1 \rangle$	\mathbf{p} not conserved without phonon or other, not a pair process	1
$\langle \omega_1 \pm 2\omega_2 \mathbf{A}(\omega_2)^2 \omega_1 \rangle$	\mathbf{p} not conserved without phonon or other, not a pair process	1
$\langle \omega_1 \pm \omega_2 V_3 \omega_1; \omega_2 \rangle$	allowed as a pair-pair process	0
$\langle \omega_1 \pm 2\omega_2 \overrightarrow{V_2} \omega_1; \omega_2 \rangle$	two step pair-pair process	0
$2\psi_- \Leftrightarrow \overleftarrow{\psi}_+ + \overleftarrow{\psi}_+$	exchange of components	0

Transition to and from the vacuum state to an excited spin wave state are allowed for all ferromagnetic materials without considering phonon interactions and the scattering of thermal spin waves into a BELC. The last two transitions are between BELC scattering interaction. These four transitions have only been easily seen in well annealed iron based alloys or glasses and were not evident in nickel or cobalt under similar test conditions. Though the cobalt and nickel samples were not as well annealed as the iron specimens. These four transitions look to be from the scattering of BELC alone and not a direct interaction with the applied field. The last two transitions require a spin wave in both bands so that angular momentum is conserved. This would not be possible in either nickel or cobalt and are not seen.

The field dependent matrix elements do not seem to operate over the entire material to produce these paired states. They seemed to be limited to magnetic domain boundaries that can be perturbed by the fields. The surface of iron would not be a source of these paired spin waves because it is not a region in which the local magnetization goes through zero. To apply a surface to iron that would have this characteristic would make an enhanced source of these waves and the sample would be more sensitive to coupling with external fields without having the losses associated for a penetrating field. If a material surface is coated with a thin anti ferromagnetic layer over the iron, it maybe possible to use this new interface with the iron as an enhanced source of these paired spin waves.

CONCLUSION

With the application of a transverse time dependent induction, $\mathbf{H}(\omega)$, in iron and steel lifts the degeneracy in the phase of the magnetization of the spin wave and allows spin pairs across bands to couple forming $J = 0$ states. The reduction of a coupled pair to a $J = 0$ states within frequency ranges removes the strongest scattering interactions for the spin wave and allow its wave length to scale upwards by five order of magnitude. This is first detected by noting the effective mass of the spin wave has been scaled back by ten orders of magnitude. This leaves this new group of spin waves which are subject to Bose-Einstein

statistics at sufficient but easily achievable densities to allow a formation of a Bose-Einstein like condensation all the way to the Curie point.

Two other time dependent magnetization dispersion curves were also identified one with a coupled magneto-acoustic coupling that operates when these long wavelength spin waves have velocities below the velocity of sound and second dispersion curve found was a measure of the density of a new state that had a net zero momentum. This process of forming the BELC for the freely propagating spin waves reduced the strong spin wave coupling to lattice as whole and allows the formation of a collective zero momentum bound state. This new field ψ_- show a strong response at high frequencies and is also macroscopically large relative to the sample size. From the spatial representation of the BELC wave functions the inter particle interaction energies were computed for these two spin wave fields and are consistent from what would be expected from a stable BEC. The BELCs formed are very weakly interacting with their environment though they interact strongly with each other. Transition between BELC states of different energy enables the creation of new states.

The passage of these propagating magnetization through regions held above the Curie point is not simply explained by one field or another. Though it does appear that ψ_- preferentially traverse this region due to the phase drop. The fraction of signal in each state as a function of temperature also has to be known along with the gain as a function of temperature.

Returning to the original problem of putting Maxwell's equations into a form to handle these problems now looks to be tractable with the solutions of the Gross-Pitaevskii equations and model for BELC populations dynamics from the coupling of the field into these states and at low frequencies coupling in the elastic properties of the material. Notation is simplified by this approach to the dynamic magnetic problem. These ideas should be useful in studying other ferromagnetic materials other than iron, which may not exhibit as many features as were found here. These effects will go along way in explaining a number of measurements made in steels over the years that were not understood. But of more general interest, the mechanics of multiple BELC activity and boson mass are topics of interest in other branches of physics. The system studied here after careful analytical development may yield more insights because of the relative ease with which experiments can be done and ideas tested.

ACKNOWLEDGEMENTS

I would like to acknowledge the careful and extensive measurement of high temperature eddy current responses in a variety of steels by Mike Bergerhouse that firmly established this problem, the discussions of signal transmission and noise through steels taken above the Curie point with Michael Wallace that gave clues to the character of the radiation source, Julian Nobel for giving me an appreciation for the concept of mass and to Steven Wallace whose patient methods of attack on problems was the example I followed. Editing to reduce these data to a readable form was generously performed by Jerry Dunn and Michael Wallace.

Appendix A: Single Homogenous Reflector

The simple case of a reflector that is a magnetic conductor or insulator can be represented by a boundary value problem where the electric field and the magnetic induction are required to be continuous across the interface. The vector potential of the source field in free space

will be represented by f the reflected response will be g and the field propagating into the magnetic medium is F . The time dependence of the fields is sinusoidal, $e^{-i\omega t}$ as driven by the source. The coefficient for the field are \mathbf{a} , \mathbf{b} and \mathbf{c} to produce the three vector potentials $\mathbf{a}f$, $\mathbf{b}g$ and $\mathbf{c}F$. The electric field $\mathbf{E} = -i\omega\mathbf{A}$ and the magnetic induction $H = \frac{\nabla \times \mathbf{A}}{\mu}$. In this one dimensional representation the curl of the particular vector potential will be represented by f' , g' and F' . Dividing out the time dependence the vector potential one has the relationship for the continuity for the transverse electric field:

$$\mathbf{a}f + \mathbf{b}g = \mathbf{c}F \quad [1a]$$

similarly for the continuity of the magnetic induction:

$$\frac{\mathbf{a}f' + \mathbf{b}g'}{\mu_o} = \frac{\mathbf{c}}{\mu}F' \quad [2a]$$

We measure

$$V = \int \mathbf{E} \cdot d\mathbf{l} = -i\omega \int \mathbf{A}d\mathbf{l} \quad [3a]$$

In the normalized form of our calibration the measured reflected field is

$$V_{normalized} = -i\omega \int \frac{\mathbf{b}g}{\mathbf{a}f}d\mathbf{l} = -i\omega\Lambda \frac{\mathbf{b}g}{\mathbf{a}f} \quad [4a]$$

where Λ is a length Solving the continuity equations to eliminate \mathbf{c} and define \mathbf{b} in terms of \mathbf{a} .

$$\mathbf{a}\left\{f - \frac{\mu F}{\mu_o F'}f'\right\} = \mathbf{b}\left\{\frac{\mu F}{\mu_o F'}g' - g\right\} \quad [5a]$$

For simplicity taking the case of an infinite planar reflector at $x = 0$ with $f = e^{ikx}$, $g = e^{-ikx}$ and $F = e^{iKx}$ the above relation reduces to:

$$\frac{\mathbf{b}}{\mathbf{a}} = \frac{\mu k - \mu_o K}{\mu k + \mu_o K} \quad [6a]$$

Taking in free space $k = \omega\sqrt{\epsilon\mu_o}$ and $K = \frac{i+1}{\sqrt{2}}\sqrt{\mu\sigma\omega}$ for the conducting magnetic medium. The result simplifies where d is just a constant.

$$\frac{\mathbf{b}}{\mathbf{a}} = \frac{\mu - d\mu^{.5}}{\mu + d\mu^{.5}} = \frac{\mu^{.5} - d}{\mu^{.5} + d} \quad [7a]$$

Then in the limit of $\mu \rightarrow \infty$, $\frac{\mathbf{b}}{\mathbf{a}} \rightarrow 1$. This is true for magnetic conductor or insulator and also in the cylindrical geometry.

As a comment the two dimensional solution of a coil as a loop source surrounding a cylindrical bar taken from reference 12 equation 63 can be computed for an empty coil and one filled with one homogeneous materials. The ratio of these two integral equations can be taken in the limit of $\mu \rightarrow \infty$ to show the reflections are bounded. If the same is tried for the loop above a plane, the probe field, there is a miss print in equation 22 and 24 where the terms have not been divide by the the material permeability so that before using equation 41 this derivation has to be corrected.

BIBLIOGRAPHY

- 1 H. Rowland, Phil. Mag., **48** p. 321 (1874).
- 2 E.M. Terry Phys.Rev. **30** no. 2 p. 133 (1910).
- 3 R.M. Borzoth, J. Appl. Phys, **8** p. 575 (1937).
- 4 H. J. Williams, R. M. Bozorth, W. Shockley, Phys. Rev. **75** p. 155 (1949).
- 5 J. Sola, US Patent, **2,694,177** Nov. 9 1954.
- 6 F. Brailsford, Physical Principles of Magnetism, van Nostrand, (London) 1966.
- 7 T.R. Schmidt, Mater. Eval. **42**, no 2 p. 225 (1984).
- 8 F Block, Z.Physik **61**, p. 206 (1930); **74** p. 295 (1932).
- 9 A.Sommerfeld, H. Bethe Elektronentheorie der Metalle, Springer, Berlin 1933.
- 10 W.B. Pearson, A Handbook of Lattice Spacings and Structures of Metals and Alloys, Vol. 1, p. 908. Oxford: Pergamon Press 1967.
- 11 V.L. Moruzzi, J.F. Janak, A.R. Williams, Calculated Electronic Properties of Metals Pergamon Press p. 170 NYC 1978.
- 12 C.V. Dodd & W. E. Deeds J. Appl. Phys. **39**,2829 (1968).
- 13 L.D. Landau & E.M. Lifshitz, Electrodynamics of Continuous Media, Trans J.B. Sykes, J.S. Bell p. 120 Pergamon Press, Bristol 1960.
- 14 R. M. Siegfried, The Reconstruction of Electrical Conductivity Profiles Using Multi-frequency Eddy Current Testing, Thesis, University of Minnesota, Mnpl. Minn. 1983.
- 15 J.P. Wallace, J.K. Tien, J.A. Steffani, K.S. Choe J. Appl. Phys. **69** p. 550 (1991).
- 16 J.P. Wallace, US Patent, **4,651,094** March 17, 1987, col 12-14.
- 17 M.E. Armacanqui, Eddy Current Detection of Sensitization in Types 304 and 316 Stainless Steels. Masters Thesis Univ. Minn. 1981.
- 18 C.Iheagwara, A Study of Transformation Kinetics in Cast Iron and Slag using Eddy Current Technique, Masters Thesis Univ. Minn. 1982.
- 19 Mike Bergerhouse, private communications 1995.
- 20 G. Shirane, R. Nathens, O. Steinsvoll, H.A. Alperin, S.J. Pickart, Phys. Rev. Lett. **15** p 146 (1965).
- 21 A.I. Akhiezer, V.G. Bar'yakhtar, S.V. Peletminskii, Spin Waves trans S. Chomet trans. ed. S. Doniach, p. 134, North-Holland Pub., Amsterdam (1968).
- 22 H. Bethe, Z. Physik **61** p. 205 (1931).
- 23 S.O. Demokritov, V.E. Demidov, O. Dzyapko, G.A. Melkov, A.A. Serga, B. Hillebrands and A.N. Slavin Nature **443**, p. 430 (2006).
- 24 L.D. Landau, E. M. Lifshitz, Statistical Physics, trans E. Peierls and R.F. Peierls, Pergamon Press, London 1958.
- 25 F. Dalfovo, S. Giorgini, M. Guilleumas, L. P. Pitaevskii, S. Stringari Rev.Mod.Phys. **71**, p. 463 (1999).
- 26 A.A. Thiele Phys. Rev. B. **7** p. 391 (1973).
- 27 J.P. Wallace, Journal of Metals, **61** no. 6 p. 67 (2009).
- 28 K. Honda, S.Kaya, Sci.Rep. Tohoku Univ. **15** p. 721 (1926).
- 29 J. Schwinger Quantum Mechanics, ed. B-G. Englert, p. 321, Springer, Berlin 1965.